Ligand Binding to Heme Proteins: Connection between Dynamics and Function†

Peter J. Steinbach,‡ Anjum Ansari,‡ Joel Berendzen,§ David Braunstein, Kelvin Chu, Benjamin R. Cowen,∥ David Ehrenstein, Hans Frauenfelder,* J. Bruce Johnson, Don C. Lamb, Stan Luck, Judith R. Mourant, G. Ulrich Nienhaus, Pal Ormos,⊥ Robert Philipp, Aihua Xie, and Robert D. Young#

Department of Physics, University of Illinois at Urbana-Champaign, 1110 West Green Street, Urbana, Illinois 61801

Received August 6, 1990; Revised Manuscript Received November 26, 1990

ABSTRACT: Ligand binding to heme proteins is studied by using flash photolysis over wide ranges in time (100 ns–1 ks) and temperature (10–320 K). Below about 200 K in 75% glycerol/water solvent, ligand rebinding occurs from the heme pocket and is nonexponential in time. The kinetics is explained by a distribution, $g(H)$, of the enthalpic barrier of height H between the pocket and the bound state. Above 170 K rebinding slows markedly. Previously we interpreted the slowing as a "matrix process" resulting from the ligand entering the protein matrix before rebinding. Experiments on band III, an inhomogeneously broadened charge-transfer band near 760 nm ($\approx$13 000 cm^{-1}) in the photolyzed state (Mb*) of (carbonmonoxy)myoglobin (MbCO), force us to reinterpret the data. Kinetic hole-burning measurements on band III in Mb* establish a relation between the position of a homogeneous component of band III and the barrier H. Since band III is red-shifted by 116 cm^{-1} in Mb* compared with Mb, the relation implies that the barrier in relaxed Mb is 12 kJ/mol higher than in Mb*. The slowing of the rebinding kinetics above 170 K hence is caused by the relaxation Mb* → Mb, as suggested by Agmon and Hopfield [(1983) *J. Chem. Phys. 79*, 2042–2053]. This conclusion is supported by a fit to the rebinding data between 160 and 290 K which indicates that the entire distribution $g(H)$ shifts. Above about 200 K, equilibrium fluctuations among conformational substates open pathways for the ligands through the protein matrix and also narrow the rate distribution. The protein relaxations and fluctuations are nonexponential in time and non-Arrhenius in temperature, suggesting a collective nature for these protein motions. The relaxation Mb* → Mb is essentially independent of the solvent viscosity, implying that this motion involves internal parts of the protein. The protein fluctuations responsible for the opening of the pathways, however, depend strongly on the solvent viscosity, suggesting that a large part of the protein participates. While the detailed studies concern MbCO, similar data have been obtained for MbO_2 and CO binding to the β chains of human hemoglobin and hemoglobin Zürich. The results show that protein dynamics is essential for protein function and that the association coefficient for binding from the solvent at physiological temperatures in all these heme proteins is governed by the barrier at the heme.

The binding of small ligands to heme proteins appears to be a simple reaction, described for the particular case of carbon monoxide binding to myoglobin by the one-step scheme Mb + CO ⇄ MbCO (Antonini & Brunori, 1971). In 1975 our group showed that data taken over wide ranges in time and temperature suggest a scheme in which a CO molecule, coming from the solvent, encounters, not one, but three or four potential barriers (Austin et al., 1975). In 1983, Agmon and Hopfield (1983) introduced a model which explained the low-temperature features observed by Austin et al. and described some of the features seen at high temperatures as a relaxation process. Here we show that ligand-binding and kinetic hole-burning experiments together lead to a model in which features of the Agmon–Hopfield model are kept, but where the reaction surface becomes time and temperature dependent. The model fits the low- and the high-temperature data using two sequential barriers.

Kinetics of CO Binding to Myoglobin

(*1.1*) *Method and Results.* In a flash photolysis experiment, a laser pulse strikes an MbCO sample and breaks the bond between the CO and the heme iron. The difference in the absorption spectra at a selected wavelength, $\Delta a(t)$, for the bound and the dissociated species monitors the subsequent CO rebinding. The survival probability, $N(t,T) \equiv \Delta a(t)/\Delta a(0)$, is the fraction of Mb molecules at temperature T that have not rebound CO at the time t after the flash. We have previously described the experimental technique and the rebinding data (Austin et al., 1975; Doster et al., 1982; Dlott et al., 1983; Ansari et al., 1986). We have repeated the flash photolysis experiments with an improved system.

(*1.2*) *Reaction Energy Landscape.* CO rebinding data to sperm whale myoglobin are shown in Figure 1. We call the faster process seen at all temperatures I for "internal"; it is nonexponential in time and independent of CO concentration. The slower process that appears above 200 K, denoted by S for "solvent", is exponential in time with a rate coefficient proportional to the CO concentration in the solvent. The processes I and S can be described in terms of the reaction potential $V(\mathrm{rc})$ sketched in Figure 2 (Austin et al., 1975;

† This work was supported in part by the National Science Foundation (Grant DMB87-16476), the National Institutes of Health (Grants GM 18051 and 32455), and the Office of Naval Research (N00014-89-R-1300). G.U.N. thanks the Alexander von Humboldt Foundation for a Feodor Lynen Fellowship. R.D.Y. thanks Illinois State University for research assistance.

* To whom correspondence should be addressed.

‡ Present address: National Institutes of Health, Bethesda, MD.

§ Present address: Los Alamos National Laboratory, Los Alamos, NM.

∥ Present address: Department of Chemistry, University of Pennsylvania, Philadelphia, PA.

⊥ Permanent address: Institute of Biophysics, Hungarian Academy of Sciences, Szeged, Hungary.

Permanent address: Department of Physics, Illinois State University, Bloomington, IL.

0006-2960/91/0430-3988$02.50/0

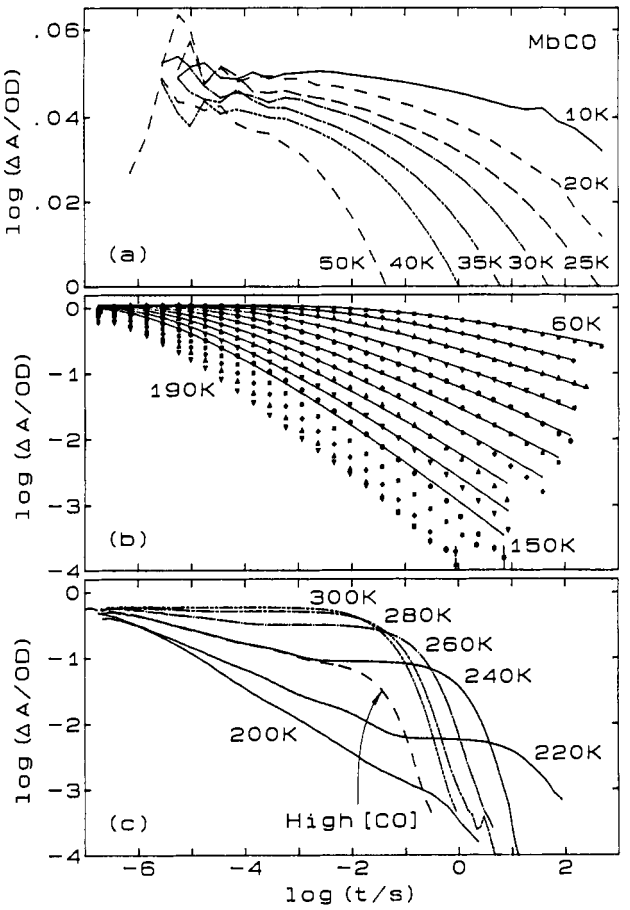

FIGURE 1: Rebinding of CO to Mb after flash photolysis. $\Delta a(t)$, the absorbance change at the time t after photodissociation, measured at 440 nm, is plotted versus log t. $\Delta a(0)$ = 1.12 OD below 200 K, pH 6.8. Solvent: 75% glycerol/buffer (v/v). CO pressure in (c): 1 bar for the high-[CO] curve and 0.05 bar for the solid curves. Note that the scale in panel a is expanded by a factor of approximately 100.

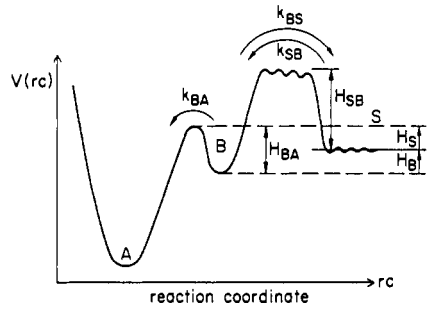

FIGURE 2: Reaction energy landscape. The bound state, MbCO, is denoted by "A". In "B", the CO is in the heme pocket. The wiggly region represents the protein matrix. "S" is the solvent.

Frauenfelder et al., 1989). In biological ligand binding, a ligand moves from the solvent, S, through the protein matrix into the heme pocket, B. From B, it can either return to the solvent or bind to the heme iron by overcoming a barrier of height H_{BA}. The bound state, MbCO, is denoted by A. In a photodissociation experiment, the protein is initially in state A. A photon breaks the Fe–CO bond, and the system moves to state B. From there, the CO can either rebind directly (process I, B → A) or move to the solvent and bind from there (process S, S → B → A). Process I has an unexpected temperature dependence: With increasing temperature it becomes faster up to about 170 K, but slows down above. To explain this behavior, we originally introduced a fourth deep well in the reaction coordinate and interpreted process I above 170 K as the "matrix process", the geminate rebinding from the protein matrix (Austin et al., 1975; Doster et al., 1982). We show in the present paper that a fourth well is not needed and that a three-well model with a time- and temperature-dependent energy landscape can explain the data.

(1.3) Static Three-Well Model. After photodissociation, the system is in well B within less than 1 ps (Petrich et al., 1988; Jongeward et al., 1988). For MbCO, thermal dissociation is negligible (k_{AB} = 0) and the solvent process S is temporally separated from the internal process I. Moreover, we have [CO] ≫ [Mb] so that k_{SB} can be written as a pseudo-first-order coefficient. Under these conditions, the survival probability $N(t,T)$ becomes (Frost & Pearson, 1953; Alberding et al., 1976b)

$$N(t,T) = N_I(t,T) + N_S(t,T) \quad (1)$$

$$N_I(t,T) = \frac{k_{BA}}{k_{BA} + k_{BS}} \exp(-\lambda_I t) \quad (2)$$

$$N_S(t,T) = \frac{k_{BS}}{k_{BA} + k_{BS}} \exp(-\lambda_S t) \quad (3)$$

$$\lambda_I = k_{BA} + k_{BS}, \quad \lambda_S = k_{SB}k_{BA}/(k_{BA} + k_{BS}) \quad (4)$$

$N_I(t,T)$ describes the internal process I and $N_S(t,T)$ the rebinding from the solvent; λ_S is the association rate coefficient.

(1.4) Conformational Substates (CS). The nonexponential time dependence of process I is caused by the existence of conformational substates (Frauenfelder et al., 1988; Elber & Karplus, 1987). Mb molecules in different CS possess different activation enthalpy barriers H_{BA}. At low temperatures, each Mb molecule remains frozen into a particular CS and $N_I(t,T)$ becomes

$$N_I(t,T) = \int dH_{BA}\, g(H_{BA}) \exp[-k_{BA}(H_{BA},T)t] \quad (5)$$

where $g(H_{BA})\, dH_{BA}$ is the temperature-independent probability for finding an Mb molecule with an activation enthalpy between H_{BA} and $H_{BA} + dH_{BA}$, and $k_{BA}(H_{BA},T)$ is the corresponding rate coefficient. Above about 50 K, $k_{BA}(H_{BA},T)$ is given by a transition-state expression (Dlott et al., 1983)

$$k_{BA}(H_{BA},T) = A_{BA}(T/T_0) \exp(-H_{BA}/RT) \quad (6)$$

where T_0 is taken to be 100 K. With eq 6, $g(H_{BA})$ is determined from a nonlinear least-squares fit of the measured $N(t,T)$ by eq 5 (Austin et al., 1975; Young & Bowne, 1984). Where we deal exclusively with process I, we drop the subscript BA on k_{BA} and H_{BA}.

The distribution $g(H)$ is related to other protein properties as outlined in Figure 3. A given substate, represented by a well in the multidimensional conformational energy landscape (Figure 3a), contributes a homogeneous component to an inhomogeneously broadened spectral line (Figure 3b) and possesses a corresponding barrier height H (Figure 3c), which results in a related rebinding rate coefficient (Figure 3d). Conformational substates are arranged in a hierarchy (Ansari et al., 1985). MbCO can assume a small number of substates of tier 0, denoted by CS0, which are characterized by different CO stretch frequencies and different angles α between the CO dipole and the heme normal (Ansari et al., 1987; Ormos et al., 1988; Hong et al., 1990). Three CS0, listed in Table I, are clearly distinguishable; they are denoted by A_0, A_1, and A_3. They rebind CO with different rates and consequently have different barriers between B and A. Rebinding after photodissociation to each individual CS0 is nonexponential in time, proving that each substate of tier 0 comprises a large number of substates of tier 1, CS1 (Ansari et al., 1987; Berendzen & Braunstein, 1990).

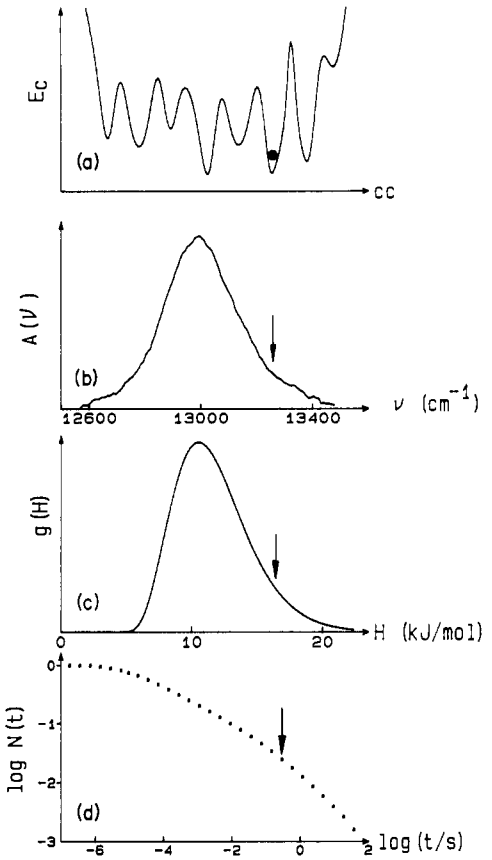

FIGURE 3: Connections among the conformational energy landscape (a), the inhomogeneously broadened spectral band III (b), the activation enthalpy distribution $g(H_{BA})$ (c), and the nonexponential rebinding $N(t,T)$ (d).

Table I: Parameters Characterizing the Three Substates of Tier 0[a]

substate	ν_{CO} (cm^{-1})	α (deg)	log [A_{BA} (s^{-1})]	H_p (kJ/mol)	Γ_H (kJ/mol)
A_0	~1966	15	8.7	8.7	6
A_1	~1945	28	8.9	10.0	7
A_3	~1927	33	10.4	18.6	9

[a] The peak frequency of the CO stretch band is denoted by ν_{CO}. α is the angle between the heme normal and the CO dipole. The activation enthalpy distribution $g(H_{BA})$ in eq 5 is described by a Gaussian with peak position H_p and width Γ_H. A_{BA} is the preexponential factor in eq 6. The values for H_p and A_{BA} are from recent unpublished experiments.

Kinetic Hole Burning

Cooper (1983) and Agmon and Hopfield (1983) pointed out that conformational substates should lead to inhomogeneous broadening of the absorption spectra of proteins. The inhomogeneity has been verified by many experiments (Ormos et al., 1986; Srajer et al., 1986). The peak, ν', of the homogeneous components of an inhomogeneously broadened band is related to the barrier height H (Sassaroli & Rousseau, 1987) as shown in Figure 3 and as verified by kinetic hole-burning experiments (Campbell et al., 1987; Agmon, 1988; Ormos et al., 1990). Here we determine $H(\nu')$ by first establishing the connection between ν' and the rebinding rate coefficient k.

(2.1) Method and Materials. To use kinetic hole burning for the study of proteins, suitable spectral markers must be found. We describe here one such marker, band III near 760 nm (≈13 000 cm^{-1}). Iizuka et al. (1974) first noticed that the band III that appears in MbCO after photodissociation (Mb*) at 4.2 K is red-shifted by about 10 nm from its position in equilibrium deoxyMb. Band III is sensitive to the local conformation near the heme iron because it is a charge-transfer transition involving iron and porphyrin states (Eaton & Hofrichter, 1981; Makinen & Churg, 1983; Chavez et al., 1990).

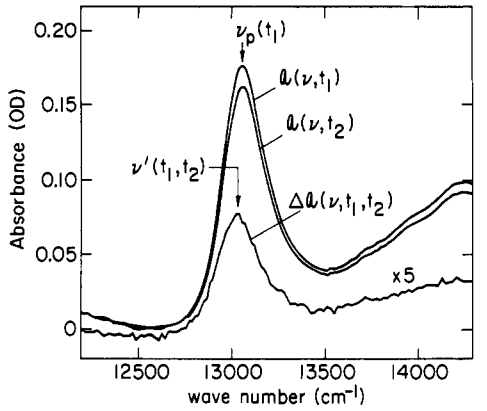

FIGURE 4: Rebinding of an inhomogeneous band. $a(\nu,t_1)$ is the average of five scans of band III taken consecutively after photodissociation of MbCO in pH 7, 75% glycerol/buffer (v/v) at 42 K. $a(\nu,t_2)$ is the average of five scans taken immediately after $a(\nu,t_1)$. The peak wavenumber $\nu'(t_1,t_2)$ of the difference spectrum $\Delta a(\nu,t_1,t_2)$ differs from $\nu_p(t_1)$.

Figure 4 shows band III in Mb* taken at two different times, t_1 and t_2, after photodissociation at 42 K. Band III occurs only in unligated Mb, and the total area is proportional to the number of unligated protein molecules. We denote the absorption spectrum measured at time t after photodissociation with $a(\nu,t)$ and the difference of the spectra measured at times t_1 and t_2 with $\Delta a(\nu,t_1,t_2) = a(\nu,t_1) - a(\nu,t_2)$. If the band is homogeneous, but the protein structure changes with time and shifts the band, $\Delta a(\nu,t_1,t_2)$ will have a derivative shape (Alben & Fiamingo, 1984). If the protein structure remains unchanged during rebinding, but the band is inhomogeneous, with the peak position of each homogeneous band component correlated with the barrier height as in Figure 3, the band will decrease nonuniformly. Band components corresponding to small barriers disappear fastest. As a consequence of a monotonic correlation, $\Delta a(\nu,t_1,t_2)$ will show a single peak with a position that depends on t_1 and t_2.

$\Delta a(\nu,t_1,t_2)$ yields an empirical correlation between the rate coefficient k for rebinding at the heme and the peak position $\nu'(t_1,t_2)$ of the relevant homogeneous component of the inhomogeneous band. We denote with $f(k)\,dk$ the probability of rebinding with rate coefficient between k and $k + dk$. The fraction of proteins with rate coefficient k that rebind between times t_1 and t_2 is

$$r(k,t_1,t_2) = \exp(-kt_1) - \exp(-kt_2) \tag{7}$$

and the average rate coefficient becomes

$$\langle k(t_1,t_2)\rangle = \int kf(k)\, r(k,t_1,t_2)\, dk \Big/ \int f(k)\, r(k,t_1,t_2)\, dk \tag{8}$$

If $kf(k)$ is a slowly varying function in the time window of the instrument,[1] $\langle k\rangle$ becomes

$$\langle k\rangle = [(1/t_1) - (1/t_2)]/\ln(t_2/t_1) \tag{9}$$

This procedure yields a unique relation between $\langle k\rangle$ and $\nu'(t_1,t_2)$. If $kf(k)$ varies appreciably, $\langle k\rangle$ can be determined numerically with eq 8. At a given temperature, Mb molecules with band position ν' rebind from the heme pocket with an average rate coefficient $\langle k(\nu')\rangle$.

[1] The probability density $f(k)$ is related to the probability density $g(\ln k)$ by $|f(k)\,dk| = |g(\ln k)\,d(\ln k)|$. Thus, $g(\ln k) = kf(k)$; $g(\ln k)$ is slowly varying if $kf(k)$ is. For an Arrhenius relation, eq 6, $\ln k$ depends linearly on the barrier H.

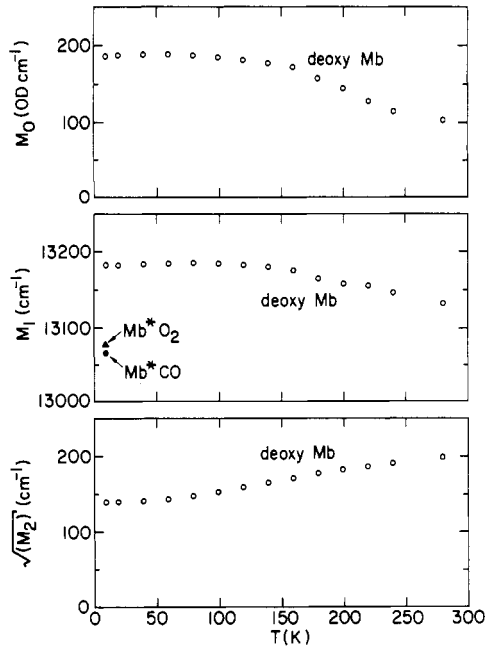

FIGURE 5: Temperature dependence of the zeroth (M_0), first (M_1), and second (M_2) moments of band III for myoglobin. The moments are defined as $M_0 = \int a(\nu)\, d\nu$, $M_1 = \int a(\nu)\nu\, d\nu/M_0$, $M_2 = \int a(\nu)\nu^2\, d\nu/M_0 - M_1^2$. $a(\nu)$ is the absorbance at the wavenumber ν. M_0 is the area under the line. M_1 measures the band position and is identical with the peak wavenumber for a symmetric line. M_2 gives a measure for the width of the line. $\sqrt{M_2}$ is equal to the parameter ω for a Gaussian line shape $a(\nu)$ = (const) $\exp[-(\nu - \nu_p)^2/2\omega^2]$. The values for Mb* at 10 K are plotted as filled symbols. The shift between the values of Mb* and deoxyMb is 116 cm^{-1} for CO and 104 cm^{-1} for O_2 in 75% glycerol/buffer solution at pH 7.

For our experiments with band III, lyophilized sperm whale metMb (Sigma Chemical Co., St. Louis, MO) was dissolved in distilled deionized water. The protein solution was centrifuged and filtered through 1.2-μm filter paper to give stock solution with a protein concentration of about 8 mM. The metMb stock was dissolved in 75% glycerol/buffer solution to give about 0.5 mM protein in 0.1 M potassium phosphate buffer (pH 7). The air above the solution was replaced with CO and N_2 for the MbCO and deoxyMb samples, respectively. Sodium dithionite solution freshly prepared under anaerobic conditions was added to the O_2-free solution to reduce the ferric iron in metMb to the ferrous form.

The extinction coefficient of band III is approximately 0.2 OD mM^{-1} cm^{-1} at 300 K, about a factor of 1000 smaller than that of the main $\pi \rightarrow \pi^*$ transition in the Soret region. A sample cell was therefore designed with a path length of 10 mm for the monitoring beam and a path length of less than 1 mm for the photolyzing light. The cell was placed inside a copper sample holder equipped with a Si temperature-sensing diode. A Lake Shore Cryotronics DRC 82C controller regulated the temperature of the block to within 0.1 K. The absorption spectra were measured with an OLIS-converted Cary 14 spectrometer interfaced to an IBM PC. The MbCO samples were photodissociated with a xenon arc lamp. A long-pass filter with cutoff at about 480 nm eliminated sample heating by the Soret line. Infrared heating was minimized by a 10-cm water filter. Illumination time for photodissociation of the sample was about 10 s. We measured band III in deoxyMb as a function of temperature. The base line was fitted by a cubic polynomial and subtracted from the spectrum. The zeroth, first, and second moments of the band are given in Figure 5.

(*2.2*) *Relaxation and Kinetic Hole Burning in Band III.* Figure 5 shows that at 10 K band III in Mb* is red-shifted by 116 cm^{-1} as compared to deoxyMb. This difference arises from different molecular geometries around the heme iron which affect the electronic transitions. At 10 K, the protein molecules cannot fully relax into the deoxy structure after photodissociation. At some higher temperature, however, the relaxation Mb* $\rightarrow$ Mb must be observable as a shift of band III from the Mb* position to that of deoxyMb. We found a shift between 60 and 160 K and interpreted it as the conformational relaxation Mb* $\rightarrow$ Mb (Ansari et al., 1985). Subsequently, Friedman and collaborators proved that the band shift is caused by kinetic hole burning and that no measurable relaxation occurs below 70 K (Campbell et al., 1987; Ansari, 1988). We will see in subsection 4.4 that the relaxation Mb* $\rightarrow$ Mb most likely starts above 170 K. Since the experiments discussed in this section are performed below 170 K, they can be interpreted in terms of kinetic hole burning alone.

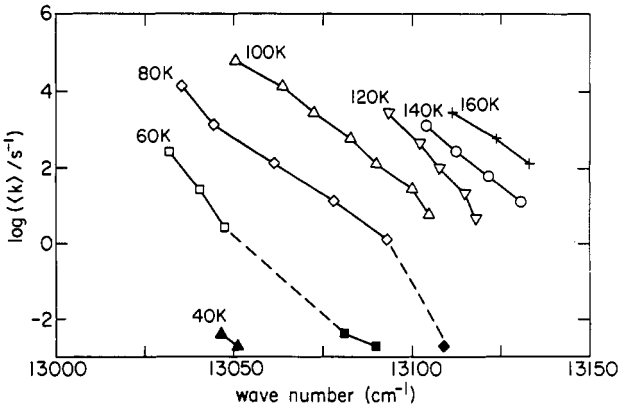

FIGURE 6: Plot of the rate coefficient $\langle k \rangle$ for binding at the heme iron versus the band position ν' of the relevant homogeneous component of band III. Filled symbols represent data taken with the OLIS–Cary 14 spectrophotometer; others represent data taken with the flash photolysis system. The data have been corrected for the temperature-dependent shift of band III (Figure 5). Uncertainties are typically less than ± 5 cm^{-1}. Sample: MbCO in 75% glycerol/buffer solution at pH 7.

(*2.3*) *Rebinding Rate and Band Position in Band III.* We have determined the difference spectra $\Delta a(\nu,t_1,t_2)$ of band III in Mb* as a function of the times t_1 and t_2 after photodissociation of MbCO over a wide range of temperature. Between 10 and 90 K, the experiments were performed in steps of 4 K on the OLIS–Cary spectrometer. After photolysis, we followed the rebinding for 1.8 ks by taking 10 successive spectra of band III. For each temperature, the difference spectrum was calculated between the averages of the first two and the last four spectra. A cubic polynomial was fitted as a base line and subtracted from the difference spectrum. The proteins that rebind between t_1 and t_2 were characterized by the first moment $\nu'(t_1,t_2)$ of the difference spectrum. The data at higher temperatures were obtained with our flash photolysis system (Ansari et al., 1985). Owing to the lower wavelength resolution, these data were fitted by Voigtian line shapes. At each temperature, the average rate coefficient, $\langle k \rangle$, was determined with eq 9. The result, shown in Figure 6, gives the connection between the rate coefficient $\langle k(T) \rangle$ and the band position ν' of the homogeneous components of band III.

Band Position and Rebinding Barrier

To connect the band position ν' to the barrier height H (H_{BA} in Figure 2), we must relate the rate coefficient k to H.

(*3.1*) *Rate Coefficient and Barrier Height.* Above about 50 K, the connection between H and k is given by eq 6 as

$$H = RT \ln (AT/kT_0) \qquad (10)$$

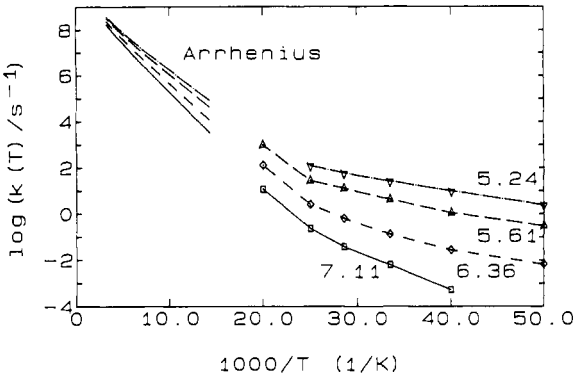

FIGURE 7: Rate coefficient $k(H,T)$ for the binding of CO at the heme iron, parametrized by the barrier height H, as a function of $10^3/T$. Data above 70 K assume an Arrhenius relation, eq 6.

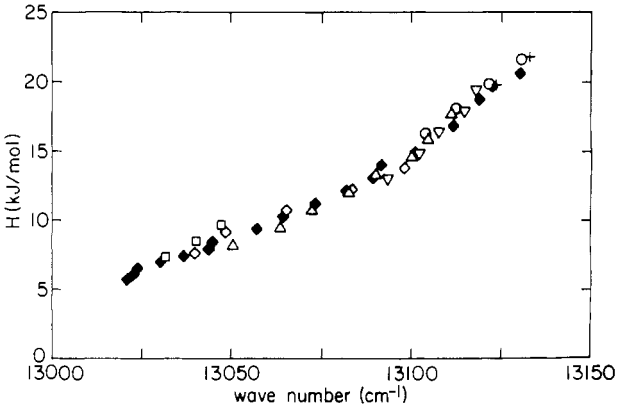

FIGURE 8: Connection between the barrier height H for the binding at the heme iron and the corresponding band position ν' of the homogeneous component of band III. Sample: MbCO in 75% glycerol/buffer solution at pH 7. Filled symbols denote data obtained from fitting the OLIS–Cary measurements; open symbols denote flash photolysis data. Uncertainties are typically less than ±5 cm^{-1}.

Below about 50 K, quantum mechanical tunneling contributes measurably to the binding of CO to heme proteins (Alberding et al., 1976a,b, 1978a,b; Alben et al., 1980). No simple expression such as eq 10 is applicable to tunneling (Hänggi et al., 1990), but the distribution of barrier heights as expressed by eq 5 permits us to determine $k(H,T)$ also in the tunneling regime (Frauenfelder, 1979). The result, $k(H,T)$ from 20 to 300 K, is given in Figure 7.

(3.2) Enthalpic Barrier H and Band Position ν′. With Figures 6 and 7, the barrier height H is determined as a function of ν'. The relation is shown in Figure 8. Low values of ν' characterize small barriers. In the models constructed to describe the binding of CO at the heme iron, the main contribution to H comes from the proximal side (Agmon & Hopfield, 1983; Young & Bowne, 1984; Srajer et al., 1988). Before binding, the iron is displaced from the mean heme plane toward the proximal side by a distance c; on binding, it moves closer to the mean heme plane (Dickerson & Geis, 1983; Kuriyan et al., 1986). In the simplest picture, H increases with c. The correlation shown in Figure 8 then implies that the position ν_p of band III also increases with increasing c. The same relation is found in Mb and Mb*: We expect Mb* to be only partially relaxed and c to be smaller than in Mb. The smaller c is accompanied by a smaller peak wavenumber, ν_p, as shown in Figure 5. A comparison of ν_p in Mb and Hb also agrees: Band III in Hb is blue-shifted by 115 cm^{-1} as compared to Mb (Iizuka et al., 1974; Cordone et al., 1986), and the distance c is larger in Hb than in Mb (Dickerson & Geis, 1983).

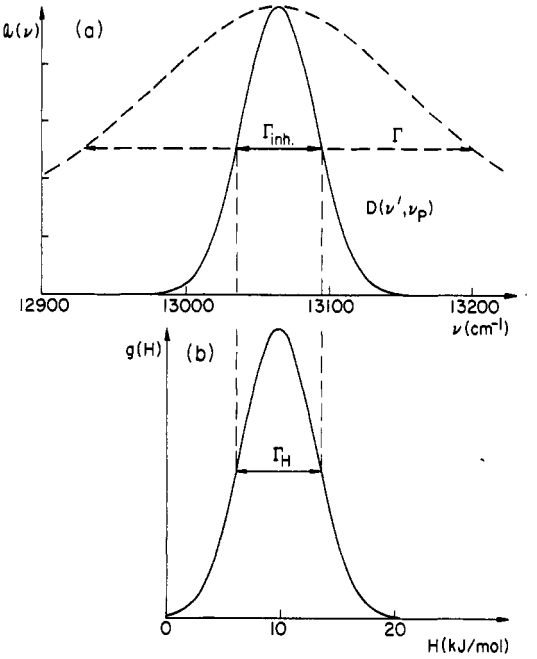

FIGURE 9: Connection between the line shape of band III and the activation enthalpy spectrum. (a) The dashed line gives the envelope (total line) of band III at low temperatures. The solid curve is the inhomogeneous distribution $D(\nu',\nu_p)$. (b) The activation enthalpy spectrum $g(H)$, determined at low temperatures.

The correlation between H and ν' can be understood in a simple model. We assume band III to be a Gaussian superposition of Lorentzians

$$a(\nu) = (\text{const}) \int D(\nu',\nu_p)\, S(\nu,\nu')\, d\nu' \qquad (11)$$

where the homogeneous contributions are described by Lorentzians $S(\nu,\nu')$ of width Γ_h centered at ν':

$$S(\nu,\nu') = (\text{const})[(\nu - \nu')^2 + \Gamma_h^2/4]^{-1} \qquad (12)$$

The inhomogeneous spectral distribution is taken to be a Gaussian of width $\Gamma_{inh} = 2(2 \ln 2)^{1/2}\omega_{inh}$, centered at ν_p:

$$D(\nu',\nu_p) = (\text{const}) \exp[-(\nu' - \nu_p)^2/2\omega_{inh}^2] \qquad (13)$$

Figure 9a shows the band envelope and the inhomogeneous distribution for values $\Gamma_{inh} = 60$ cm^{-1} and $\Gamma_h = 240$ cm^{-1}. Figure 9b gives the barrier distribution, $g(H)$, of eq 5. We approximate $g(H)$ by a Gaussian of width Γ_H centered at H_p and assume a linear mapping between $D(\nu',\nu_p)$ and $g(H)$ as indicated in Figure 9. $H(\nu')$ is then given by

$$H(\nu') = H_p + (\Gamma_H/\Gamma_{inh})(\nu' - \nu_p) \qquad (14)$$

Such a linear relation is to be expected if H and the charge-transfer transition depend similarly on the out-of-plane distance c of the iron atom. A linear relation between the barrier height and a protein coordinate is also displayed in Figure 3 of the paper by Agmon and Hopfield (1983). The data in Figure 8 are linear between about 5 and 15 kJ/mol and show a change in slope above 15 kJ/mol. The change may be caused by the fact that rebinding of CO at values of H up to about 15 kJ/mol is dominated by the substate A_1. Above about 15 kJ/mol the substate A_3 dominates (Ansari et al., 1987; Berendzen & Braunstein, 1990). A fit of eq 14 to the data between 5 and 15 kJ/mol in Figure 8 gives $\Gamma_H/\Gamma_{inh} = 0.11 \pm 0.01$ kJ/mol cm^{-1}.

Protein Relaxation and CO Binding

(4.1) A Prediction. Figure 8 and eq 14 relate the barrier height $H(\nu')$ for the binding of CO at the heme iron to the

band position ν' of the corresponding homogeneous component of band III. Figure 5 shows that at pH 7 band III shifts by $\Delta\nu_r = 116\ cm^{-1}$ upon the relaxation Mb* → Mb. The two facts combined imply that H shifts by

$$\Delta H = (\Gamma_H/\Gamma_{inh})\Delta\nu_r \quad (15)$$

in going from Mb* to Mb. With the value $\Gamma_H/\Gamma_{inh} = 0.11$ kJ/mol cm^{-1} and $\Delta\nu_r = 116\ cm^{-1}$, we get $\Delta H = 12 \pm 1$ kJ/mol for the dominant substate A_1. The relaxation of the protein should increase the barrier height. The estimate given here depends on the assumption that the shift $\Delta\nu_r$ is temperature independent.

The increase of the barrier height upon the relaxation Mb* → Mb can explain the behavior of process I above 170 K. Figure 1 shows that process I speeds up as the temperature is increased from 10 to 170 K. Above 170 K, process I becomes slower. The connection between ΔH and $\Delta\nu_r$ suggests that the relaxation Mb* → Mb starts near 170 K and causes the slowdown. In order to test this hypothesis and to characterize the temperature dependence of process I quantitatively, we consider protein motions.

(*4.2*) *Protein Motions—General Features.* Two types of protein motions are relevant for ligand binding (Ansari et al., 1985). In equilibrium fluctuations (EF), a protein hops from substate to substate. EF0, for instance, denotes fluctuations among the three CS0. Functionally important motions (FIM) are nonequilibrium motions. They occur in protein reactions or can be induced by perturbations, for instance, temperature or pressure jumps: The protein starts out in a nonequilibrium state and approaches equilibrium with a time dependence characterized by a relaxation function $\Phi(t,T)$. $\Phi(t,T)$ for a particular property $O(t)$ is defined by

$$\Phi(t,T) = [O(t,T) - O(\infty,T)]/[O(0,T) - O(\infty,T)] \quad (16)$$

Relaxation phenomena in glasses (Zallen, 1983; Brawer, 1985; Jäckle, 1986) and in proteins (Iben et al., 1989; Frauenfelder et al., 1990) display two significant properties, a nonexponential time dependence and a non-Arrhenius temperature dependence. The time dependence can be approximated by a stretched exponential

$$\Phi(t,T) = \exp\{-[\kappa(T)t]^{\beta}\} \quad (17)$$

where $\kappa(T)$ is a rate coefficient[2] and the Kohlrausch–Williams–Watts exponent β lies between 0 and 1. Experiments in many systems indicate that β is essentially temperature independent over a wide range (Jäckle, 1986).

The temperature dependence of rate coefficients is usually described by an Arrhenius relation. For many processes in glasses and in proteins eq 6 is inappropriate as can be seen by looking at the preexponential factor A. A value of A very much larger than $10^{13}\ s^{-1}$ implies unphysically large reaction rates at high temperatures and suggests the use of a different relation. We employ the simplest expression that approximates relaxation data in amorphous systems (Ferry et al., 1953):

$$\kappa(T) = A \exp[-(E/RT)^2] \quad (18)$$

Equation 18 has been derived for a random walk of an excitation within a Gaussian density of states (Bässler, 1987; Zwanzig, 1988; Bryngelson & Wolynes, 1989; Richert & Bässler, 1990). Equation 18 fits the data well over an extended temperature range, but at temperatures well above the glass transition, $\kappa(T)$ is smaller than eq 18 predicts. Within a narrow interval around a given temperature T, eq 18 can be approximated by an Arrhenius relation, with a "local activation enthalpy"

$$H_{loc}(T) = 2E^2/RT \quad (19)$$

(*4.3*) *Motions Involved in Ligand Binding.* After photodissociation the protein relaxes toward the deoxy structure (Henry et al., 1985; Ansari et al., 1985; Rousseau & Argade, 1986; Sassaroli et al., 1986; Petrich et al., 1990). The first step involves only the heme group. Initially, the iron is close to the mean heme plane. Within less than 100 fs after photodissociation, the distance $c(t)$ between the iron and the mean heme plane changes from the bound-state value $c(0) \approx 0$ to a value $c(0^+) \approx 0.3$ Å. Molecular dynamics calculations by Karplus and collaborators (Petrich et al., 1991) provide details for this scenario and indicate that the initial relaxation at room temperature occurs in about 50 fs.

As the temperature increases above 170 K, large-scale motions set in (Iben et al., 1989; Frauenfelder et al., 1990) and three dynamic processes influence ligand binding: (i) The Mb* structure relaxes to the deoxy structure, the iron moves from the frozen position $c(0^+)$ to the deoxy equilibrium position $c(\infty)$, and the band III blue shifts by $116\ cm^{-1}$. (ii) A protein in a given CS0 fluctuates among CS1; we denote these fluctuations by EF1. (iii) Each Mb molecule fluctuates (EF0) among the substates A_0, A_1, and A_3. The rates for the EF0 and EF1 are not yet known, but the fluctuation–dissipation theorem (Kubo, 1966) implies that the rates for EF*i* and FIM*i* must be similar. Limits on EF0 are given by NMR and IR experiments (Fiamingo et al., 1986). At room temperature, a 75-MHz NMR measurement yields a single Lorentzian, indicating that the exchange among the CS0 is faster than a few microseconds. IR measurements show well-resolved CO stretch bands. The widths of these bands are about $10\ cm^{-1}$; the exchange must consequently be slower than about 10 ps.

(*4.4*) *The Relaxation Mb* → Mb.* We consider first the relaxation Mb* → Mb in which process I slows as the barrier H_{BA} increases. In analogy to the relaxation phenomena in glasses, we describe the change in H_{BA} by a relaxation function $\Phi^*(t,T)$ and write

$$H_{BA}(t,T) = H_0 + \Delta H^*_{BA}[1 - \Phi^*(t,T)] \quad (20)$$

where t is the time after photodissociation. The rate coefficient for CO rebinding, eq 6, becomes time dependent:

$$k_{BA}(H(t,T),T) = A_{BA}(T/T_0) \exp[-H_{BA}(t,T)/RT] \quad (21)$$

The differential equation for binding, $dN_1(t,T) = -k_{BA}(H(t,T),T)\, N_1(t,T)\, dt$, leads to the survival probability $N_1(t,T)$ for a single barrier $H_{BA}(t,T)$:

$$N_1(t,T) = \exp\left[-\int_0^t dt'\, k_{BA}(H(t',T),T)\right] \quad (22)$$

The survival probability for a protein ensemble becomes

$$N_1(t,T) = \int dH_0\, g(H_0) \exp\left[-\int_0^t dt'\, k_{BA}(H(t',T),T)\right] \quad (23)$$

Equation 23 is valid if $k_{BA} \gg k_{BS}$. This condition holds below about 220 K. The distribution function $g(H_0)$ is time and temperature independent, but the rate coefficient $k_{BA}(H(t',T),T)$ depends on time. As relaxation function $\Phi^*(t,T)$, we use eq 17 with $\kappa^*(T)$ given by eq 18. The fit of eq 23 to the data up to 210 K yields $\Delta H^*_{BA} \approx 11$ kJ/mol, $A^* \approx 10^{18}\ s^{-1}$, $E^* \approx 10$ kJ/mol, and $\beta^* = 0.24$. The coefficient $\kappa^*(T)$ is shown in Figure 10, and the fit is given in Figure 11. The model describes the behavior of process I between 160 and 210 K very well, and ΔH^*_{BA} agrees with the value of $\Delta H = 12$

[2] We denote the rate coefficients for reactions as in eqs 2–4 by k and λ, and those for relaxation processes by κ.

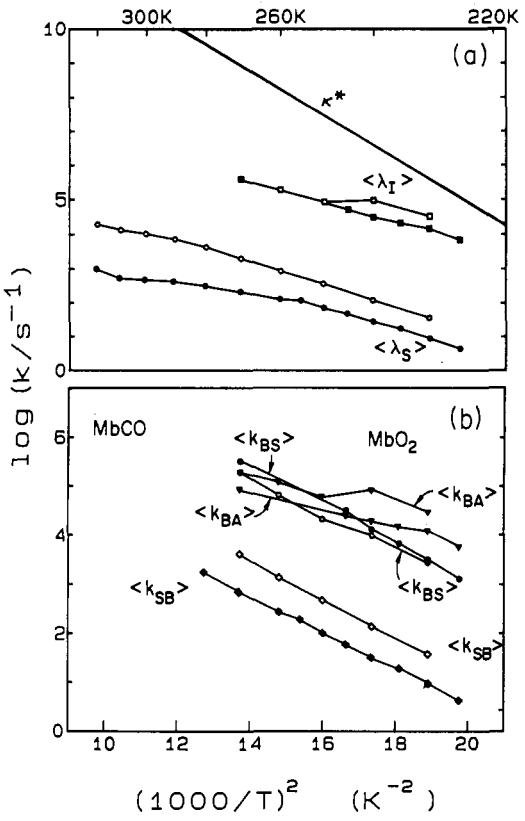

FIGURE 10: Plot of rate coefficients versus $(1000/T)^2$ for MbCO (solid symbols) and MbO_2 (open symbols). Solvent: 75% glycerol/buffer, pH 6.6–7. Details are discussed in the text. Note that the CO data refer to a pressure of 1 bar, and the O_2 data to a pressure of 0.2 bar. For equal O_2 and CO pressures, the $\langle\lambda_S\rangle$ and $\langle k_{SB}\rangle$ for O_2 would be shifted up by a factor of 5, indicating that O_2 enters the pocket about 12 times faster than CO.

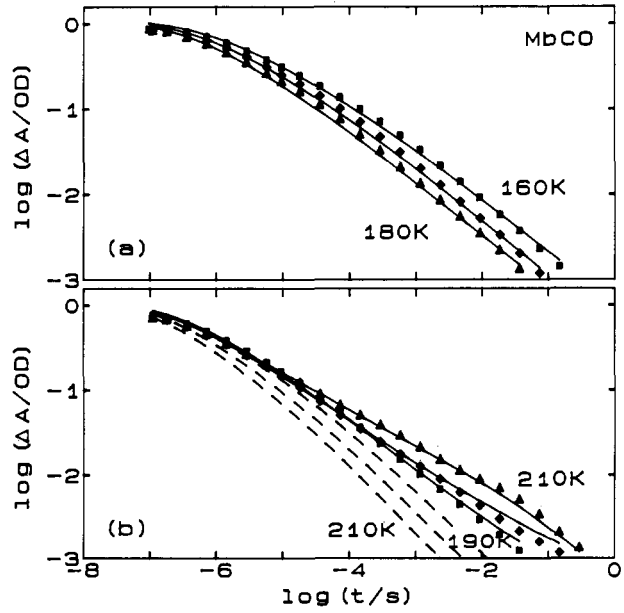

FIGURE 11: Data and fit to the relaxation model for MbCO from 160 to 210 K. The *solid lines* show the fit with the *relaxation* Mb* → Mb taken into account by using eq 23. (a) Internal process I at 160–180 K. (b) Process I at 190–210 K. The *dashed lines* give the prediction for process I if *no relaxation* Mb* → Mb occurs.

kJ/mol obtained from the shift of the band III. The extrapolation to room temperature gives $\kappa^*(293\text{ K}) \approx 5 \times 10^{10}\text{ s}^{-1}$, consistent with the observations that the resonance Raman spectrum of Mb* is not relaxed within 30 ps (Dasgupta et al., 1985) and that band III has shifted to the deoxy position by

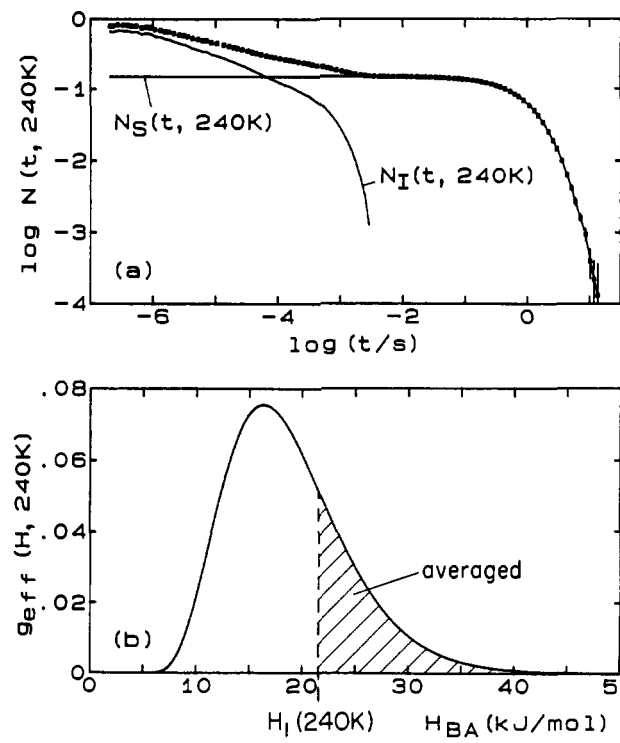

FIGURE 12: (a) The measured survival probability $N(t,240\text{ K})$ for the rebinding of CO to Mb is decomposed into the exponential contribution $N_S(t,240\text{ K})$ from the solvent process and the internal rebinding process $N_I(t,240\text{ K})$. (b) Distribution function $g_{eff}(H,T)$ at 240 K. The entire $g_{eff}(H,T)$ is partially relaxed and hence shifted to higher H_{BA} than in Figure 3c. Proteins in substates with $H_{BA} < H_I(T)$ have rebinding rates k_{BA} faster than $(1/\tau_I)$. They rebind before hopping to another substate. Proteins in the shaded part $H_{BA} > H_I(T)$ have rebinding rates slower than $(1/\tau_I)$ and fluctuate from CS to CS; their ligands can either move into the solvent or rebind.

10 ns (Sassaroli & Rousseau, 1987). The relaxation function $\Phi^*(t,293\text{ K})$, calculated with the parameters given above, is consistent with the molecular dynamics computation of the iron motion by Karplus and collaborators (Petrich et al., 1991). Similar relaxation processes have been observed by Friedman (1985) in hemoglobin. The parameters for the rate coefficient $\kappa^*(T)$ are similar to those for glass relaxations. The value of β^* demonstrates that the shift is nonexponential in time. We justify the use of eq 18 for the temperature dependence by also fitting the data around $T = 200$ K to an Arrhenius relation. The result, $A \approx 10^{33}\text{ s}^{-1}$ and $E \approx 120$ kJ/mol, implies that an Arrhenius relation is inappropriate.

(4.5) Effects of Equilibrium Fluctuations.[3] Figure 1 shows that a new phenomenon sets in above 200 K: Some of the photodissociated CO molecules escape into the solvent. Molecular dynamics simulations show that the escape of the CO molecules requires a fluctuating protein (Case & Karplus, 1979; Elber & Karplus, 1990). Rebinding from the solvent is approximately exponential in time, $N_S(t,T) = N_S(0,T)\exp(-\lambda_S t)$. Subtracting $N_S(t,T)$ from $N(t,T)$ yields $N_I(t,T)$, shown in Figure 12a for $T = 240$ K. $N_I(t,T)$ characterizes the geminate rebinding from the pocket. For rebinding to a single CS0, $N_I(t,T)$ is nonexponential in time to the time τ_I

[3] Semantic confusion between relaxation and fluctuation is easy, and we plead guilty to having misused the names in earlier papers. Relaxation denotes the approach to equilibrium from a nonequilibrium state. Fluctuations are equilibrium motions (EF) among conformational substates. If the EF are fast compared to the observed phenomena, the measured observables are fluctuationally averaged, meaning that the distribution collapses to a single value. In NMR, this effect is known as motional narrowing.

Table II: Parameters Characterizing the Association Reaction in Four Heme Proteins in 75% Glycerol/Buffer Solution[a]

	data at 300 K[b]		data at low T		relaxation Mb* → Mb (κ^*)[d]			
system	λ_S ($\times 10^3$ s^{-1})	H_S (kJ/mol)	H_p (kJ/mol)	log [A_{BA} (s^{-1})]	β^*	E^* (kJ/mol)	log [A^* (s^{-1})]	ΔH^a_{BA} (kJ/mol)
MbCO	0.5	12	9.7 ± 0.4	8.8 ± 0.2	0.24 ± 0.06	10 ± 1	18 ± 3	11 ± 1
MbO_2	6.5	≈20	9.2 ± 0.6	8.9 ± 0.3	0.14	9 ± 2	11	9.9
LbCO[c]	5.9	≈20	5.3 ± 0.8	9.0 ± 0.5	0.22 ± 0.1	9.5 ± 2	16	14
β^ACO	1.1	≈20	3.6 ± 0.2	9.5	0.45	8 ± 2	13 ± 3	11 ± 1
β^{ZH}CO	8	≈20	2.3 ± 0.3	9.1	0.56	6.3 ± 1.5	11 ± 3	12 ± 1

[a] Parameters are defined in the text. Errors reflect ~50% increase in χ^2 of the fit. [b] Ligand pressure 1 atm. [c] Lb = soybean leghemoglobin (Stetzkowski et al., 1985). [d] Errors omitted exceed 50% of the best value.

and then drops off approximately exponentially. The drop-off is caused by the escape of CO molecules into the solvent and by the averaging over the distribution of rate coefficients k_{BA}. We assume that both effects are caused by the same equilibrium fluctuations, EF1, which we characterize by an average rate coefficient $\langle \kappa_1(T) \rangle$ and set

$$\langle \kappa_1(T) \rangle \approx 1/\tau_1 \tag{24}$$

All observations are consistent with this choice. If $\langle \kappa_1(T) \rangle$ were much larger than $1/\tau_1$, $N_1(t,T)$ would become exponential at a time shorter than τ_1. If $\langle \kappa_1)T) \rangle$ were much smaller than $1/\tau_1$, $N_1(t,T)$ would continue to be nonexponential beyond τ_1.

The effect of the EF1 can be discussed with Figure 12b, which shows the effective activation enthalpy distribution, $g_{eff}(H,T)$ at 240 K. Mb molecules with small barriers H_{BA} rebind before their barriers have shifted appreciably; Mb molecules with large barriers rebind slowly and their barriers increase more. The effective distribution hence shifts to higher enthalpies and broadens as is indicated in Figure 12b. The distribution is divided into a white and a shaded part at the activation enthalpy $H_1(T)$, given by

$$H_1(T) = RT \ln (A_{BA}T/\langle \kappa_1 \rangle T_0) \tag{25}$$

Proteins belonging to the white part rebind the photodissociated CO with a rate coefficient $k_{BA} > \langle \kappa_1(T) \rangle$. They experience no equilibrium fluctuations, and $N_1(t,T)$ is given by eq 23. The parameters listed in Table II fit the nonexponential part of $N_1(t,T)$ up to 290 K. The distribution of activation enthalpies shifts with time up to 290 K, but the shape of the distribution remains essentially unchanged.

Proteins in the shaded part experience EF1 with an average rate coefficient $\langle \kappa_1(T) \rangle$ that is larger than k_{BA} and k_{BS}. These proteins fluctuate among the CS1, and their ligands either rebind or escape into the solvent. The ratio of the intensities of these competing processes is given by

$$N_1^{fa}(0,T)/N_S(0,T) = \langle k_{BA}(T) \rangle / \langle k_{BS}(T) \rangle \tag{26}$$

$N_1^{fa}(0,T) + N_S(0,T)$ is the fraction of proteins in the shaded part of $g_{eff}(H,T)$. The superscript fa denotes "fluctuationally averaged". $N_1^{fa}(0,T)$ is the fraction that rebinds from the heme pocket, and $N_S(0,T)$ is the fraction that loses the ligand to the solvent; $\langle k_{BA}(T) \rangle$ and $\langle k_{BS}(T) \rangle$ are the average rate coefficients for rebinding and escape of the proteins belonging to the shaded part of $g_{eff}(H,T)$. The ligand may not escape after a single fluctuation, and we set

$$\langle k_{BS}(T) \rangle = c\langle \kappa_1(T) \rangle, \qquad c < 1 \tag{27}$$

Further treatment depends on the characteristics of the equilibrium fluctuations EF1, and we discuss two extreme cases.

(i) We first assume that the EF1 lead randomly from a given H_{BA} to any other one within the entire $g_{eff}(H,T)$ in Figure 12b, but most likely to substates with $H_{BA} \approx H_p$. At temperatures below about 250 K, $k_{BA}(H_p) \gg \langle \kappa_1(T) \rangle$ so that the ligand rebinds after the conformational fluctuation with a rate coefficient approximately given by $\langle \kappa_1(T) \rangle$. For case i we consequently get with eqs 26 and 27

$$N_1^{fa}(0,T)/N_S(0,T) \approx 1/c \tag{28}$$

(ii) In the second limit, we assume that the EF1 connect only substates with similar activation enthalpies H_{BA} so that with eqs 26 and 27

$$N_1^{fa}(0,T)/N_S(0,T) \approx \langle k_{BA}(T) \rangle / c\langle \kappa_1(T) \rangle \tag{29}$$

In case i, $N_1^{fa}(0,T)/N_S(0,T)$ is approximately temperature independent; in case ii, it is a strong function of T, because we expect $\langle k_{BA}(T) \rangle$ and $\langle \kappa_1(T) \rangle$ to have very different activation enthalpies at high temperatures. A crude evaluation of the data by inspection shows that the ratio in eq 26 is temperature dependent, and hence case i is excluded. The EF1 predominantly connect substates that are close in activation enthalpies H_{BA}. We assume for simplicity that the averaging effect is restricted to substates within the shaded part of $g_{eff}(H,T)$ and write with eq 4

$$\langle \lambda_1(T) \rangle = \langle k_{BA}(T) \rangle + \langle k_{BS}(T) \rangle \tag{30}$$

Equations 26 and 30 together give

$$\begin{aligned} \langle k_{BA}(T) \rangle &= \langle \lambda_1(T) \rangle / [1 + N_S(0,T)/N_1^{fa}(0,T)] \\ \langle k_{BS}(T) \rangle &= \langle \lambda_1(T) \rangle / [1 + N_1^{fa}(0,T)/N_S(0,T)] \\ \langle k_{SB}(T) \rangle &= \langle \lambda_S(T) \rangle / [1 - N_S(0,T)] \end{aligned} \tag{31}$$

The factor in the expression for $\langle k_{SB}(T) \rangle$ arises because ligands entering the pocket bind with probability $[1 - N_S(0,T)]$. For a single substate of tier 0, eq 31 can be evaluated by determining τ_1 from the nonexponential part of $N_1(t,T)$, and $\langle \lambda_1 \rangle$, from the nearly exponential drop-off. The existence of multiple substates of tier 0, however, complicates the extraction of the relevant rate parameters, and a better technique, described in the following subsection, is needed.

(4.6) Extraction of the Rate Coefficients. The properties of the substates of tier 0 in MbCO are listed in Table I. At pH 7, where the present measurements were made, the substates A_1 and A_3 are relevant. To evaluate the rebinding data above 200 K, we use the maximum entropy method to invert $N(t,T)$ at each temperature to obtain a distribution function $f(\log \lambda, T)$, where λ is an effective rate coefficient (Steinbach, 1990):

$$N(t,T) = \int \mathrm{d}(\log \lambda)\, f(\log \lambda, T) \exp(-\lambda t) \tag{32}$$

Figure 13a shows the rate coefficient spectrum $f(\log \lambda, 230\ \mathrm{K})$, plotted versus $-\log \lambda$. Since we do not have rebinding data at times shorter than 10^{-7} s, $f(\log \lambda, T)$ for $\log \lambda > 7$ is undetermined.

Four peaks stand out in Figure 13a. Peaks 1 and 4 can be interpreted unambiguously. Peak 1 corresponds to the white part of $g_{eff}(H,T)$ in Figure 12b and represents proteins where the distribution has partially or completely relaxed, but where no averaging has taken place. Ligands in this part do not

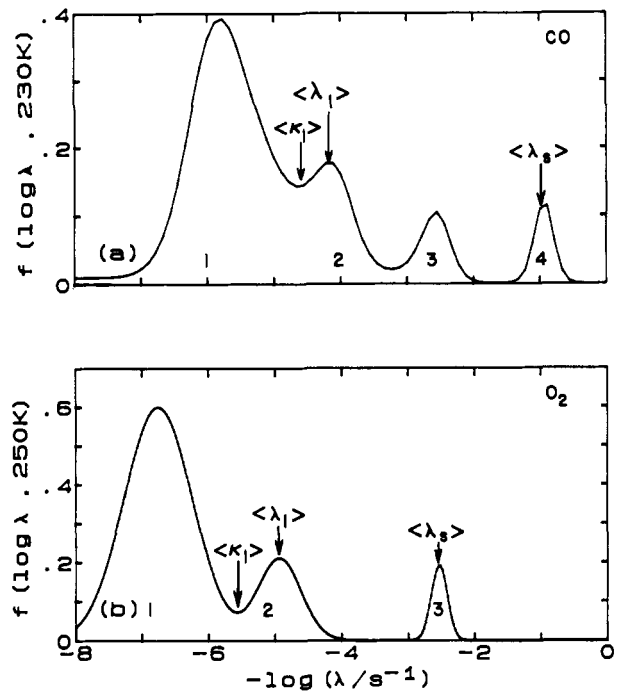

FIGURE 13: Distribution functions $f(\log \lambda,T)$ for the rebinding of CO to Mb for (a) CO at 230 K and (b) O_2 at 250 K. Data were obtained with monitoring in the visible (440 nm).

escape into the solvent, but rebind with a nonexponential time dependence. The rate coefficient $\langle\lambda_S\rangle$ of the narrow peak 4 is proportional to the CO concentration: Peak 4 represents the solvent process and belongs to the shaded part of the distribution in Figure 12b.

The interpretation of peaks 2 and 3 is more difficult. They are narrower than peak 1 and belong to the shaded part of $g_{eff}(H,T)$. Ligands corresponding to these peaks can either rebind or escape into the solvent. But why are there two peaks, and which one determines $\langle\lambda_I\rangle$? A possible interpretation is to assign peak 2 to rebinding to substrate A_1 and peak 3 to A_3. Flash photolysis experiments with separate monitoring of substates A_1 and A_3 eliminate this possibility: Both substates contribute to all peaks. Two observations compel us to assume that peak 2 determines $\langle\lambda_I(T)\rangle$: In MbO_2 (Figure 13b and subsection 5.3), peak 3 is absent and escape must involve peak 2. Moreover, at 280 K where peaks 1 and 2 are small, peak 3 is still clearly recognizable. The assignments indicated in Figure 13 yield the rate coefficients $\langle\lambda_I(T)\rangle$ and $\langle\lambda_S(T)\rangle$ shown in Figure 10a. With $N_I^{fa}(0,T)$ and $N_S(0,T)$ determined by the areas of the peaks 2 and 4, eq 31 give the coefficients $\langle k_{BA}(T)\rangle$, $\langle k_{BS}(T)\rangle$, and $\langle k_{SB}(T)\rangle$ plotted in Figure 10b. Extrapolation of $\langle k_{BA}(T)\rangle$ to 293 K yields a value of 3×10^5 s^{-1}. A check on the data and the evaluation is afforded by comparing this value with a result of Henry et al. (1983). Henry et al. measured the rebinding of CO to Mb in an aqueous solvent at room temperature and found two exponential components. By evaluating their data with a three-well model, they obtained (in our notation) $\langle k_{BA}(295\ K)\rangle = 2.3 \times 10^5\ s^{-1}$. Our extrapolation is in very good agreement with their direct measurement, providing further support for the model and the assignment of $\langle\lambda_I\rangle$ to peak 2. The unsolved problem, identification of peak 3, will require additional experiments. The discussion also shows that it can be difficult to extract $\langle\lambda_I(T)\rangle$ from a plot as in Figure 12a. The function $f(\log \lambda,T)$, eq 32, provides a more powerful tool for the data evaluation.

Figure 10 is not a standard Arrhenius plot. Even with eq 19 the slopes do not yield local activation enthalpies, because some of the rate coefficients are averages only over the shaded part of $g_{eff}(T)$ with a temperature-dependent border $H_1(T)$. The slopes give correct Arrhenius parameters in the high-temperature limit, where the averaging extends over the entire distribution.

(4.7) CO Binding to Mb at Room Temperature. Of particular interest is the rebinding at room temperature, where nearly all CO molecules move into the solvent after photodissociation. This fact implies that the relaxation Mb* → Mb is completed before any ligands rebind and that the EF0 and EF1 cover the entire relaxed distribution. In our model the fully relaxed distribution has the same shape as the one determined below 170 K (Figure 3) but is shifted by ΔH^*_{BA}. We approximate the distribution $g(H_{BA})$ by a Gaussian of width Γ_H peaked at $H_p + \Delta H^*_{BA}$. The CO molecules entering the pocket from the solvent face a rapidly fluctuating barrier. The probability of the CO in the pocket encountering a barrier of height H_{BA} is given by $g(H_{BA})$, and the fluctuationally averaged rate coefficient is given by

$$\langle k_{BA}\rangle = \int dH_{BA}\, g(H_{BA})\, k_{BA}(H_{BA},T) \qquad (33)$$

Inserting eqs 20 and 21 with $t \to \infty$ into eq 33 and performing the integration give

$$\langle k_{BA}(T)\rangle = k_{BA}(H_p + \Delta H^*_{BA},T) \exp[\Gamma_H^2/16(\ln 2)(RT)^2] \qquad (34)$$

where $k_{BA}(H_p + \Delta H^*_{BA},T)$ is the rate coefficient in eq 6, with the barrier $H_p + \Delta H^*_{BA}$ corresponding to the peak of the fully shifted distribution. Equation 34 shows that the equilibrium fluctuations cause the rate to be larger than $k_{BA}(H_p + \Delta H^*_{BA},T)$ and that the increase is determined by the width Γ_H of the enthalpy distribution. We define an effective barrier $H_{eff}(T)$ by

$$\langle k_{BA}(T)\rangle = A_{BA}(T/T_0) \exp[-H_{eff}(T)/RT] \qquad (35)$$

Equation 34 results in a simple relation for the effective barrier in the fully relaxed and fluctuationally averaged protein near 300 K:

$$H_{eff}(T) = H_p + \Delta H^*_{BA} - \Gamma_H^2/(16 \ln 2)RT \qquad (36)$$

The effective barrier lies below the one corresponding to the peak of the fully shifted distribution. The values of $H_p = 10$ kJ/mol, $\Gamma_H = 7$ kJ/mol, and $\Delta H^*_{BA} = 11$ kJ/mol (Table II) give $H_p + \Delta H^*_{BA} = 21$ kJ/mol and $H_{eff} = 19$ kJ/mol. With these parameters, we obtain $\langle k_{BA}(293\ K)\rangle = 3 \times 10^5\ s^{-1}$, in agreement with the measured value.

Experimental information on the barrier height H_{BA} in the fully relaxed and fluctuationally averaged protein comes from the temperature dependence of the association rate coefficient $\langle\lambda_S\rangle$, shown in Figure 10. Near 300 K, essentially all CO molecules move into the solvent after photodissociation, and $\langle\lambda_S\rangle$ is given by (Austin et al., 1975)

$$\langle\lambda_S\rangle = A_S \exp(-H_S/RT) \qquad (37)$$

As indicated in Figure 2, H_S [called E_{1V} in Austin et al. (1975)] is the barrier between the solvent and the top of the barrier between B and A. Experimentally, Austin et al. found $H_S = 12 \pm 1$ kJ/mol. To compare this value with H_{eff}, we note that H_{eff} characterizes the total barrier height H_{BA}, given by

$$H_{BA} = H_S + H_B \qquad (38)$$

H_B is the binding enthalpy of the CO in the heme pocket. Equations 36–38 give $H_B = 7$ kJ/mol. Supporting evidence for a weak binding exists. The frequencies of the CO stretch bands in the B substates deviate from the free CO value (Alben

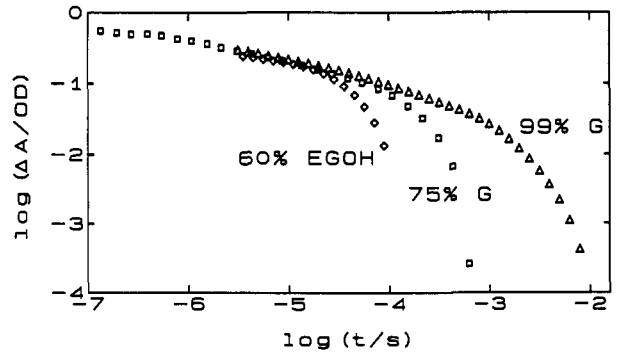

FIGURE 14: Viscosity dependence of the rebinding of CO to Mb at 250 K. The rebinding function $N_I(t,T)$ for process I is shown for three different solvents.

et al., 1982). Molecular dynamics calculations imply that the CO in the heme pocket is weakly bound (Case & Karplus, 1979). Fitting the rate coefficients $\langle k_{BS}(T)\rangle$ and $\langle k_{SB}(T)\rangle$ in Figure 10b by eq 18 yields the values E_{BS} = 8.3 kJ/mol, $A_{BS} = 4 \times 10^{11}$ s^{-1}, and E_{SB} = 7.6 kJ/mol, $A_{SB} = 8 \times 10^{7}$ s^{-1}. With eq 19 we find that the activation enthalpy for the step B → S is about 7 ± 3 kJ/mol larger than for S → B, indicating also that the CO is weakly bound in the heme pocket.

(4.8) Effect of Viscosity. The viscosity dependence of CO binding to Mb, shown in Figure 1 of the paper by Beece et al. (1980), gives additional insight into the relaxation and fluctuation phenomena. Similar data have been obtained by Findsen et al. (1988) for CO binding to Hb. In Beece et al. we explained the solvent dependence by assuming a matrix process and invoking a modified Kramers equation. In the present model both the relaxation Mb* → Mb and the motion responsible for the opening of the barrier B ↔ S can depend on viscosity. The effect of the viscosity on κ^* and κ_1 can be seen by looking at $N_I(t,T)$ at a given temperature in solvents of different viscosities. To do so, we have taken the data from Figure 1 of Beece et al. and subtracted the solvent process. Figure 14 shows the rebinding data for the internal process of MbCO in three different solvents at 250 K. The nonexponential components are nearly identical; the solvent viscosity has little or no effect on the relaxation Mb* → Mb. Measurements with MbCO embedded in ice and in solid poly(vinyl alcohol) (Austin et al., 1975; Figures 4 and 5) strengthen this observation: With the solvent frozen ($\eta \to \infty$), no solvent process occurs, but process I shows the same general behavior as in the three solvents in Figure 14. These results support the present model; the motion of the iron from $c(0^+)$ to $c(\infty)$ is an internal process, controlled at and close to the heme. The iron atom possibly remains fixed with respect to the overall protein, but the heme group domes and moves or slides away from the F helix (Kuczera et al., 1990).

The drop-off of the geminately rebinding population in Figure 14 is markedly different for the three different solvents. The data agree with the change of the fluctuation rate κ_1 among CS1 due to the different viscosities. The viscosity dependence can be parametrized by a power law (Beece et al., 1980):

$$\kappa(\eta) = \kappa_0(T)(\eta/\eta_0)^{-\mu} \qquad (39)$$

The rebinding data suggest an exponent $\mu(\kappa_1) \approx 0.5$. The equilibrium fluctuations EF1 depend on the solvent viscosity and consequently must involve a major part of the protein. Doster (1983) explains a coefficient $\mu \approx 0.5$ in a model where the fluctuation spectrum comprises two components, a solvent-independent diffusion of local structural defects and global fluctuations coupled to the solvent.

Dynamics and Function

The features discussed so far for the binding of CO to Mb occur in nearly all the heme protein systems that we have studied. In this section we provide additional examples.

(5.1) Control of Ligand Binding. Figure 2 implies that the association rate, $\langle\lambda_S\rangle$, can be controlled in two places, at the entrance to the pocket (S → B) and at the heme iron (B → A). To find a criterion for the rate-limiting step, we consider first a static reaction potential with fixed and single-valued barriers. The association rate then is given by eq 4, and we can distinguish two limiting cases:

$$\text{(i)}\quad \langle k_{BA}\rangle \gg \langle k_{BS}\rangle,\quad \langle\lambda_S\rangle \approx \langle k_{SB}\rangle,\quad N_S(0,T) \ll 1 \qquad (40)$$

$$\text{(ii)}\quad \langle k_{BA}\rangle \ll \langle k_{BS}\rangle,\quad \langle\lambda_S\rangle \approx (\langle k_{SB}\rangle/\langle k_{BS}\rangle)\langle k_{BA}\rangle,\quad N_S(0,T) \approx 1 \qquad (41)$$

In the first case, the entrance to the pocket governs the association. In the second case, binding is affected by two factors, the equilibrium coefficient (pocket occupation factor) $P_B = \langle k_{SB}\rangle/\langle k_{BS}\rangle$ and $\langle k_{BA}\rangle$, the rate coefficient for binding at the heme (Doster et al., 1982).

In the present model, two quantities indicate if case i or ii holds, $N_S(0,T)$ and the local activation enthalpy H_S of $\langle\lambda_S\rangle$. In case i, $N_S(0,T)$ will be small and H_S will be of the order of H_{SB} (Figure 2). In case ii, $N_S(0,T)$ will be close to 1 and H_S will be of the order of H_{BA}, considerably smaller than H_{SB}. We assume here that $\langle k_{BS}\rangle$ and $\langle k_{SB}\rangle$ are both governed by the same equilibrium fluctuations and hence have the same activation enthalpies.

As an example, we consider these criteria for MbCO. Figure 1c shows that $N_S(0,T) < 0.1$ below 240 K, and Figure 18 of Austin et al. (1975) indicates that $H_S > 70$ kJ/mol below about 250 K. Both criteria for case i are satisfied, and CO binding to Mb below about 250 K is governed by the passage through the protein matrix into the heme pocket. At 300 K, however, $N_S(0,T) \approx 1$ and H_S = 12 kJ/mol. Both values satisfy the criteria for case ii; binding at 300 K is governed by the barrier at the heme and the pocket occupation factor P_B.

The curves for $\langle k_{BS}\rangle$ and $\langle k_{SB}\rangle$ in Figure 10 have nearly the same slope, supporting the concept that the same motion, EF1, is responsible for the entrance and exit of the CO molecules. Entrance and exit are dynamic phenomena: The protein acts as a gate, and the ligands can pass only if the gate is open (Beece et al., 1980; Stein et al., 1989). The collective nature of the fluctuations is apparent from a fit of $\langle k_{SB}(T)\rangle$ to an Arrhenius relation; the result E = 56 kJ/mol, $A = 10^{14}$ s^{-1}, signals a complex process and implies that eq 6 is inappropriate. A fit to eq 18 yields E = 7.6 kJ/mol and $A = 8 \times 10^{7}$ s^{-1}. We symbolize the cooperative nature of the transition between B and S by the wiggly top of the barrier between pocket and solvent in Figure 2.

(5.2) Binding of CO to β^A and β^{ZH}. The binding of CO to the separated β chains of human hemoglobin poses a puzzle: The barrier at the heme is very small at low temperatures (H_p = 3.6 ± 0.2 kJ/mol), and such a barrier cannot control the binding at room temperature (Alberding et al., 1978a; Ansari et al., 1986). The model introduced here solves the puzzle. A fit to the data in Figures 3 and 4 of Ansari et al. with eq 23 reproduces process I above 170 K well. The fit parameters in Table II show that the barrier in the relaxed protein is much larger near 300 K than below 170 K and controls CO binding. A hole-burning experiment on band III verifies the shift of H_p.

Clear evidence for the existence of a "frozen" and "shifted" nonexponential process I at 300 K comes from experiments

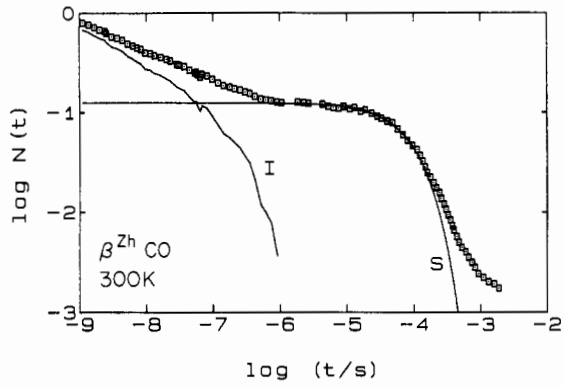

FIGURE 15: Rebinding of CO to β^{ZH} at 300 K [after Dlott et al. (1983)]. The rebinding function $N(t,300\ K)$ is decomposed into the process I and S. Solvent: 75% glycerol/buffer at pH 7.

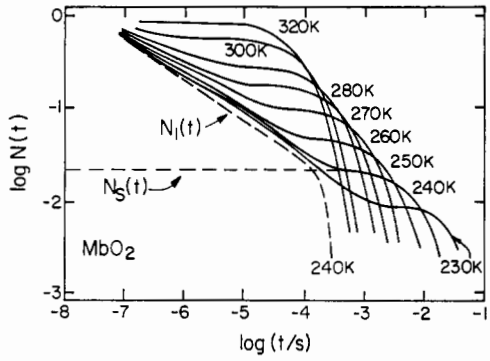

FIGURE 16: Binding after photodissociation of O_2 to Mb. Solvent: 75% glycerol/buffer, pH 7, O_2 pressure 0.2 bar [after Beece (1983)].

on the separated β chains of hemoglobin Zürich (Dlott et al., 1983). In β^{ZH}, His E7 is replaced by Arg: The arginine does not fit into the pocket and moves out of the way. The binding properties are changed dramatically. The barrier H_{BA} below about 200 K is described by a distribution with H_p = 2.3 kJ/mol and a width Γ_H = 2 kJ/mol. The rebinding data at 300 K in Figure 15 can be explained by a shifted barrier with the parameters listed in Table II plus a solvent process.

(5.3) Binding of Dioxygen to Myoglobin. The binding of O_2 to Mb is surrounded by controversy, with three paramount questions: (i) Is the binding transition B → A at the heme iron adiabatic for O_2 and CO (Frauenfelder & Wolynes, 1985) or adiabatic for O_2 but nonadiabatic for CO (Jortner & Ulstrup, 1979; Redi et al., 1981)? (ii) Is the binding controlled at the heme as we have claimed (Doster et al., 1982) or at the entrance to the pocket (Gibson et al., 1986; Jongeward et al., 1988; Sato et al., 1990; Chance et al., 1990)? (iii) Why is O_2 binding to Mb at room temperature 30 times faster than CO binding (Parkhurst, 1979)?

Before answering these questions, we describe the salient experimental features. After flash photolysis, CO shows two rebinding processes, I and S (Figure 1). O_2 also has these two processes but in addition displays a "picosecond process" I*. We discuss here first the slower processes I and S, shown in Figure 16 (Beece, 1983). The corresponding low-temperature data are given in Austin et al. (1975). The determination of the parameters for the relaxation Mb* → Mb is performed as for MbCO, and they are listed in Table II. The determination of the rate coefficients $\langle k_{BA}(T)\rangle$, $\langle k_{BS}(T)\rangle$, and $\langle k_{SB}(T)\rangle$ is plagued by a problem. IR spectroscopic studies (Potter et al., 1987) and pressure experiments (Frauenfelder et al., 1990) imply that MbO_2 has substates of tier 0, just like MbCO. In MbCO, the CS0 can be studied in detail because the CO stretch frequencies are easily measurable. The O_2 stretch spectrum is much harder to observe, and we have not yet been able to use it to get information on the CS0. A definitive identification of the CS0 and a determination of the separate activation enthalpy distributions are not yet available. We obtain some insight by using the data from Figure 16 to compute $f(\log \lambda, T)$ as in Figure 13b. Three peaks appear: The slowest is the solvent peak and the fastest is similar to peak 1 in MbCO. The intermediate peak is similar to peak 2 in Figure 13a. Data evaluation as in subsection 4.6 yields the rate coefficients given in Figure 10.

Figures 1, 10, 11, and 16 and the data in Table II permit a comparison of the binding of CO and O_2 to Mb. The general features are similar, but the relaxation of Mb* → Mb occurs faster in Mb*(CO) than in Mb*(O_2). The difference can be seen by comparing the curves for $N_I(t)$ at 240 K in Figures 11 and 16. The relaxed process I is about 10 times faster for O_2 than for CO. The difference can also be seen at 210 K: Rebinding of CO at 210 K is slower than at 190 K (Figure 11), while no such reversal occurs for O_2. With increasing T, process I always becomes faster for O_2, but the rate of the increase is less than predicted from low temperatures. The effect of the ligand on the relaxation Mb* → Mb is caused by structural differences. While the iron is in the mean heme plane in MbCO, it stays away 0.2 Å in MbO_2 (Kuriyan et al., 1986; Phillips, 1980). The work required to move the iron to the fully relaxed position about 0.35 Å away from the mean heme plane (Phillips, 1981; Nienhaus, 1987) thus is expected to be smaller in the case of Mb*(O_2); the relaxation may proceed more slowly and the total change, ΔH^*_{BA}, in activation enthalpy may be smaller for O_2 than for CO.

Process I above 170 K, visible in Figure 9 of Austin et al. (1975), has been rediscovered a few times at room temperature and denoted as "nanosecond recombination" [e.g., Gibson et al. (1986)]. The "nanosecond" optical spectra of Mb*(CO) differ from those of the deoxy form (Sato et al., 1990), consistent with the present model. We assert that the nanosecond process is the relaxing process I. A "picosecond" process, with a rate coefficient of about 10^{10} s^{-1} (Martin et al., 1982; Jongeward et al., 1988; Petrich et al., 1991), has been interpreted as rebinding of O_2 to a nonrelaxed and still planar heme. We have seen a similar but slower process, denoted by I*, in the binding of CO to carboxymethylated cytochrome c (Alberding et al., 1978b) and to HRP (Doster et al., 1987). We interpret I* as fast rebinding to an iron still in the heme plane.

We can now answer question i. Following photodissociation we distinguish binding before and after the iron has moved out of the heme plane from $c(0)$ to $c(0^+)$. At $c(0)$ the steric barrier is probably very small. If the iron stays in plane for a sufficiently long time, both O_2 and CO can rebind via process I*. O_2 will bind adiabatically and fast, CO nonadiabatically and about 2 orders of magnitude slower. This situation occurs in CM (carboxymethylated) cyt c and HRP, where the protein structure probably slows the movement $c(0) \rightarrow c(0^+)$. In Mb, the initial out-of-plane motion of the iron is very fast and only O_2 can bind through process I*. With the iron out of plane, a much higher steric barrier controls binding, and O_2 and CO both bind adiabatically as is demonstrated by the nearly equal values of their preexponential factors A_{BA} (Table II). Indeed, the rate coefficients $\langle k_{BA}(T)\rangle$ in Figure 10b show that O_2 binds only about 3 times faster than CO to the heme iron, further supporting the notion that both bind adiabatically.

To answer question ii, we distinguish between the rebinding after photodissociation and binding from the solvent to deoxyMb. After photodissociation, a major fraction of O_2 will never move into the solvent but will rebind from the heme

pocket via process I*. In the physiological binding of O_2 to Mb, the heme is already in the deoxy structure, with the iron out of plane. We expect that binding is the same as in process S in flash photolysis. Figure 10b shows that $\langle k_{BS} \rangle$ is larger than $\langle k_{BA} \rangle$ at 300 K. Process S for MbO_2 at physiological temperatures is close to the limiting case ii, and $\langle \lambda_S \rangle$ is given by eq 41. A look at the activation enthalpies leads to the same conclusion. The effective barrier H_S for process S near 300 K is of the order of 20 kJ/mol, far smaller than the activation enthalpy for $\langle k_{SB}(T) \rangle$ at 300 K, about 70 kJ/mol. Stopped-flow experiments at room temperature by Antonini and co-workers (Antonini & Brunori, 1971) also give an activation enthalpy of about 25 kJ/mol for the O_2 binding to Mb, only consistent with control at the heme. The results agree with the work of Lakowicz and Weber (1973) and Jameson et al. (1984), who found that O_2 diffuses rapidly through the protein matrix.

The answer to question iii comes from the data in Figure 10b and eq 41. Figure 10b shows that the main difference between CO and O_2 is the rate coefficient $\langle k_{SB} \rangle$ for entering the pocket. For equal gas pressure (1 bar), O_2 enters about 12 times faster than CO but leaves slightly slower. The equilibrium coefficient (pocket occupation factor) P_B is consequently about 20 times larger for O_2 than for CO. These data suggest that the dominant property leading to a faster dioxygen binding is its "higher solubility" in the heme pocket. The effective barrier H_{eff} and $\langle k_{BA} \rangle$ are about the same for O_2 and CO. The rate $\langle k_{BA} \rangle$ sets an upper limit for the association rate coefficient $\langle \lambda_S \rangle$. Thus $\langle \lambda_S \rangle$ is controlled by proximal effects. The stationary pocket properties (P_B) reduce the association rate from the limit determined by $\langle k_{BA} \rangle$. Thus distal effects are responsible for the discrimination between O_2 and CO.

Summary and Conclusions

(6.1) The Model. The binding of CO and O_2 to Mb is governed by two barriers (Figure 2). The inner barrier is located at the heme iron. Up to 160 K the rebinding of ligands after flash photolysis can be described by a temperature-independent distribution of enthalpic barriers $g(H_{BA})$. The rate coefficient $k_{BA}(T)$ satisfies an Arrhenius equation and is independent of the solvent viscosity. Above 160 K, the barrier distribution shifts by about 10 kJ/mol to higher enthalpies. We interpret the shift as being caused by the relaxation Mb* → Mb. The relaxation function $\Phi^*(t,T)$ is nonexponential in time (eq 17), non-Arrhenius in temperature (eq 18) and essentially independent of the solvent viscosity. At room temperature the barrier H_{BA} is still distributed, but equilibrium fluctuations (EF1) result in average rate coefficients $\langle k_{BA} \rangle$.

The outer barrier between the solvent S and the heme pocket B is formed by the protein matrix. Above 210 K we observe transitions S ↔ B which can be visualized as a migration of the ligand through the fluctuating protein molecule. The rate coefficient $\kappa_1(T)$ for these equilibrium fluctuations (EF1) possesses a non-Arrhenius temperature dependence and is strongly viscosity dependent. At temperatures between 210 and 250 K and/or high solvent viscosity, the ligand binding kinetics is dominated by the outer barrier. At room temperature and moderate viscosity, the inner barrier controls.

The new model is simpler than the earlier four-well version (Austin et al., 1975). It connects experimental observations from flash photolysis kinetics, kinetic hole burning, and pressure jump relaxations. While only the association reactions of CO and O_2 to myoglobin are discussed in detail in this paper, the new model also applies to other heme proteins. The resulting parameters are summarized in Table II.

(6.2) Hierarchy of Substates and Motions. Binding involves a number of substates and motions. Substates of tier 0 (CS0) are present in heme proteins (Table I) and must be included in a detailed picture of ligand binding. The CS1 give rise to distributed barriers H_{BA} within a given CS0; fluctuations among the CS1 substates permit the passage of ligands through the protein matrix and are responsible for the exponential time dependence of the binding from the solvent. We assign to tier 2 the motions that are responsible for the relaxation Mb* → Mb and the shift of the activation enthalpy spectrum $g(H_{BA})$ after photodissociation.

The identification of the tiers with structural features is tentative. We essentially follow Rousseau and Argade (1986) in assuming that FIM 2 represents the motion of the iron from its position immediately after photolysis to the deoxy equilibrium position. The fluctuations EF1 may involve motions of the F helix (Friedman, 1985). An even larger part of the protein molecule may participate in the EF0.

(6.3) A Brief Comparison of Models. In our model, the relaxation Mb* → Mb and the fluctuations among conformational substates with different enthalpic barriers H_{BA} belong to two different tiers (CS2 and CS1). This separation is forced upon us by the experimental data. It leads to a time- and temperature-dependent energy landscape. The seminal paper by Agmon and Hopfield (1983) restricts the discussion to a single tier; hence it cannot reproduce the experimental data in detail and leads to a value H_S (Figure 2b) that is too high. Young and Bowne (1984) did not include the relaxation Mb* → Mb and obtain a value of H_S that is too low. Srajer et al. (1988) introduce two protein coordinates, but the motions along these coordinates are coupled. An extension of the models will be necessary for a more complete comparison between experiment and theory.

Acknowledgments

We thank N. Agmon, R. H. Austin, M. Karplus, and P. G. Wolynes for helpful discussions and comments. R.D.Y. thanks S. Van Roekel for computer programming and assistance. Part of this paper was written at the Aspen Center for Physics (H.F.).

References

Agmon, N. (1988) *Biochemistry 27*, 3507–3511.

Agmon, N., & Hopfield, J. J. (1983) *J. Chem. Phys. 79*, 2042–2053.

Alben, J. O., & Fiamingo, F. G. (1984) in *Optical Techniques in Biological Research* (Rousseau, D., Ed.) Academic Press, New York.

Alben, J. O., Beece, D., Bowne, S. F., Eisenstein, L., Frauenfelder, H., Good, D., Marden, M. C., Moh, P. P., Reinisch, L., Reynolds, A. H., & Yue, K. T. (1980) *Phys. Rev. Lett. 44*, 1157–1160.

Alben, J. O., Beece, D., Bowne, S. F., Doster, W., Eisenstein, L., Frauenfelder, H., Good, D., McDonald, J. D., Marden, M. C., Moh, P. P., Reinisch, L., Reynolds, A. H., Shyamsunder, E., & Yue, K. T. (1982) *Proc. Natl. Acad. Sci. U.S.A. 79*, 3744–3748.

Alberding, N., Austin, R. H., Beeson, K. W., Chan, S. S., Eisenstein, L., Frauenfelder, H., & Nordlund, T. M. (1976a) *Science 192*, 1002–1004.

Alberding, N., Austin, R. H., Chan, S. S., Eisenstein, L., Frauenfelder, H., Gunsalus, I. C., & Nordlund, T. M. (1976b) *J. Chem. Phys. 65*, 4701–4711.

Alberding, N., Chan, S. S., Eisenstein, L., Frauenfelder, H., Good, D., Gunsalus, I. C., Nordlund, T. M., Perutz, M. F., Reynolds, A. H., & Sorensen, L. B. (1978a) *Biochemistry 17*, 43–51.

Alberding, N., Austin, R. H., Chan, S. S., Eisenstein, L., Frauenfelder, H., Good, D., Kaufmann, K., Marden, M., Nordlund, T. M., Reinisch, L., Reynolds, A. H., Sorensen, L. B., Wagner, G. C., & Yue, K. T. (1978b) *Biophys. J. 24*, 319–334.

Ansari, A. (1988) Ph.D. Dissertation, University of Illinois at Urbana–Champaign.

Ansari, A., Berendzen, J., Bowne, S. F., Frauenfelder, H., Iben, I. E. T., Sauke, T. B., Shyamsunder, E., & Young, R. D. (1985) *Proc. Natl. Acad. Sci. U.S.A. 82*, 5000–5004.

Ansari, A., Di Iorio, E. E., Dlott, D., Frauenfelder, H., Iben, I. E. T., Langer, P., Roder, H., Sauke, T. B., & Shyamsunder, E. (1986) *Biochemistry 25*, 3139–3146.

Ansari, A., Berendzen, J., Braunstein, D., Cowen, B. R., Frauenfelder, H., Hong, M. K., Iben, I. E. T., Johnson, J. B., Ormos, P., Sauke, T. B., Scholl, R., Schulte, A., Steinbach, P. J., Vittitow, J., & Young, R. D. (1987) *Biophys. Chem. 26*, 337–355.

Antonini, E., & Brunori, M. (1971) *Hemoglobin and Myoglobin in Their Reactions with Ligands*, North-Holland, Amsterdam.

Austin, R. H., Beeson, K. W., Eisenstein, L., Frauenfelder, H., & Gunsalus, I. C. (1975) *Biochemistry 14*, 5355–5373.

Bässler, H. (1987) *Phys. Rev. Lett. 58*, 767–770.

Beece, D. (1983) Ph.D. Dissertation, University of Illinois at Urbana–Champaign.

Beece, D., Eisenstein, L., Frauenfelder, H., Good, D., Marden, M. C., Reinisch, L., Reynolds, A. H., Sorensen, L. B., & Yue, K. T. (1980) *Biochemistry 19*, 5147–5157.

Berendzen, J., & Braunstein, D. (1990) *Proc. Natl. Acad. Sci. U.S.A. 87*, 1–5.

Brawer, S. A. (1985) *Relaxation in Viscous Liquids and Glasses*, American Ceramic Society, Columbus, OH.

Bryngelson, J., & Wolynes, P. G. (1989) *J. Phys. Chem. 93*, 6902–6915.

Campbell, B. F., Chance, M. R., & Friedman, J. M. (1987) *Science 238*, 373–376.

Case, D. A., & Karplus, M. (1979) *J. Mol. Biol. 132*, 343–368.

Chance, M. R., Courtney, S. H., Chavez, M. D., Ondrias, M. R., & Friedman, J. M. (1990) *Biochemistry 29*, 5537–5545.

Chavez, M. D., Courtney, S. H., Chance, M. R., Kiula, D., Nocek, J., Hoffman, B. M., Friedman, J. M., & Ondrias, M. R. (1990) *Biochemistry 28*, 4844–4852.

Cooper, A. (1983) *Chem. Phys. Lett. 99*, 305–309.

Cordone, L., Cupane, A., Leone, M., & Vittrano, E. (1986) *Biophys. Chem. 24*, 259–275.

Dasgupta, S., Spiro, T. G., Johnson, C. K., Dalickas, G. A., & Hochstrasser, R. M. (1985) *Biochemistry 24*, 5295–5297.

Dickerson, R. E., & Geis, I. (1983) *Hemoglobin*, pp 50 and 51, Benjamin/Cummings Publishing Co., Menlo Park, CA.

Dlott, D. D., Frauenfelder, H., Langer, P., Roder, H., & Di Iorio, E. E. (1983) *Proc. Natl. Acad. Sci. U.S.A. 80*, 6239–6243.

Doster, W. (1983) *Biophys Chem. 17*, 97–103.

Doster, W., Beece, D., Bowne, S. F., Di Iorio, E. E., Eisenstein, L., Frauenfelder, H., Reinisch, L., Shyamsunder, E., Winterhalter, K. H., & Yue, K. T. (1982) *Biochemistry 21*, 4831–4839.

Doster, W., Bowne, S. F., Frauenfelder, H., Reinisch, L., & Shyamsunder, E. (1987) *J. Mol. Biol. 194*, 299–312.

Eaton, W. A., & Hofrichter, J. (1981) *Methods Enzymol. 76*, 175–261.

Elber, R., & Karplus, M. (1987) *Science 235*, 318–321.

Elber, R., & Karplus, M. (1990) *J. Am. Chem. Soc. 112*, 9161–9175.

Ferry, J. D., Grandine, L. D., Jr., & Fitzgerald, E. R. (1953) *J. Appl. Phys. 24*, 911–916.

Fiamingo, F. G., Altschuld, R. A., & Alben, J. O. (1986) *J. Biol. Chem. 261*, 12976–12987.

Findsen, E. W., Friedman, J. M., & Ondrias, M. R. (1988) *Biochemistry 27*, 8719–8724.

Frauenfelder, H. (1979) in *Tunneling in Biological Systems* (Chance, B., et al., Eds.) pp 627–649, Academic Press, New York.

Frauenfelder, H., & Wolynes, P. G. (1985) *Science 229*, 337–345.

Frauenfelder, H., Parak, F., & Young, R. D. (1988) *Annu. Rev. Biophys. Biophys. Chem. 17*, 451–479.

Frauenfelder, H., Steinbach, P. J., & Young, R. D. (1989) *Chem. Scr. 29A*, 145–150.

Frauenfelder, H., Alberding, N. A., Ansari, A., Braunstein, D., Cowen, B. R., Hong, M. K., Iben, I. E. T., Johnson, J. B., Luck, S., Marden, M. C., Mourant, J. R., Ormos, P., Reinisch, L., Scholl, R., Schulte, A., Shyamsunder, E., Sorensen, L. B., Steinbach, P. J., Xie, A.-H., Young, R. D., & Yue, K. T. (1990) *J. Phys. Chem. 94*, 1024–1037.

Friedman, J. M. (1985) *Science 228*, 1273–1280.

Frost, A. A., & Pearson, R. G. (1953) *Kinetics and Mechanisms*, John Wiley & Sons, New York.

Gibson, Q. H., Olson, J. S., McKinnie, E. R., & Rohlfs, R. J. (1986) *J. Biol. Chem. 261*, 10228–10239.

Hänggi, P., Talkner, P., & Borkovec, M. (1990) *Rev. Mod. Phys. 62*, 251–341.

Henry, E. R., Sommer, J. H., Hofrichter, J., & Eaton, W. A. (1983) *J. Mol. Biol. 166*, 443–451.

Henry, E. R., Levitt, M., & Eaton, W. A. (1985) *Proc. Natl. Acad. Sci. U.S.A. 82*, 2034–2038.

Hong, M. K., Braunstein, D., Cowen, B. R., Frauenfelder, H., Iben, I. E. T., Mourant, J. R., Ormos, P., Scholl, R., Schulte, A., Steinbach, P. J., Xie, A.-H., & Young, R. D. (1990) *Biophys. J. 58*, 429–436.

Iben, I. E. T., Braunstein, D., Doster, W., Frauenfelder, H., Hong, M. K., Johnson, J. B., Luck, S., Ormos, P., Schulte, A., Steinbach, P. J., Xie, A. H., & Young, R. D. (1989) *Phys. Rev. Lett. 62*, 1916–1919.

Iizuka, T., Yamamoto, H., Kotani, M., & Yonetani, T. (1974) *Biochim. Biophys. Acta 371*, 1715–1729.

Jäckle, J. (1986) *Rep. Prog. Phys. 49*, 171–231.

Jameson, D., Gratton, E., Weber, G., & Alpert, B. (1984) *Biophys. J. 45*, 795–803.

Jongeward, K. A., Magde, D., Taube, D. J., Marsters, J. C., Traylor, T. G., & Sharma, V. S. (1988) *J. Am. Chem. Soc. 110*, 380–387.

Jortner, J., & Ulstrup, J. (1979) *J. Am. Chem. Soc. 101*, 3744–3754.

Kubo, R. (1966) *Rep. Prog. Phys. 29*, 255–284.

Kuczera, K., Kuriyan, J., & Karplus, M. (1990) *J. Mol. Biol. 213*, 351–373.

Kuriyan, J., Wilz, S., Karplus, M., & Petsko, G. A. (1986) *J. Mol. Biol. 192*, 133–154.

Lakowicz, J. R., & Weber, G. (1973) *Biochemistry 12*, 4171–4179.

Makinen, M. W., & Churg, A. K. (1983) in *Iron Porphyrins, Part I* (Lever, A. B. P., & Gray, H. B., Eds.) pp 141–235, Addison-Wesley, Reading, MA.

Martin, J. L., Migus, A., Poyart, C., Lecarpentier, Y., Antonetti, A., & Orszag, A. (1982) *Biochem. Biophys. Res. Commun. 107*, 803–810.

Nienhaus, G. U. (1987) Ph.D. Dissertation, Universität Münster.
Ormos, P., Braunstein, D., Hong, M. K., Lin, S. L., & Vittitow, J. (1986) in *Biophysical Studies of Retinal Proteins* (Ebrey, T. G., Frauenfelder, H., Honig, B., & Nakanishi, K., Eds.) pp 238–247, University of Illinois Press, Urbana, IL.
Ormos, P., Braunstein, D., Frauenfelder, H., Hong, M. K., Lin, S. L., Sauke, T. B., & Young, R. D. (1988) *Proc. Natl. Acad. Sci. U.S.A. 85*, 8492–8496.
Ormos, P., Ansari, A., Braunstein, D., Cowen, B. R., Frauenfelder, H., Hong, M. K., Iben, I. E. T., Sauke, T. B., Steinbach, P. J., & Young, R. D. (1990) *Biophys. J. 57*, 191–199.
Parkhurst, L. (1979) *Annu. Rev. Phys. Chem. 30*, 503–546.
Petrich, J. W., Poyart, C., & Martin, J. L. (1988) *Biochemistry 27*, 4049–4060.
Petrich, J. W., Lambry, J.-C., Kuczera, K., Karplus, M., Poyart, C., & Martin, J.-L. (1991) *Biochemistry* (preceding paper in this issue).
Phillips, S. E. V. (1980) *J. Mol. Biol. 142*, 531–554.
Phillips, S. E. V. (1981) *The X-ray Structure of Deoxy-Mb (pH 8.5) at 1.4 Å Resolution*, Brookhaven Protein Data Bank.
Potter, W. T., Tucker, M. P., Houtchens, R. A., & Caughey, W. S. (1987) *Biochemistry 29*, 4699–4707.
Redi, M. H., Gerstman, B. S., & Hopfield, J. J. (1981) *Biophys. J. 35*, 471–484.
Richert, F., & Bässler, H. (1990) *J. Phys.: Condens. Matter 2*, 2273–2288.
Rousseau, D., & Argade, P. V. (1986) *Proc. Natl. Acad. Sci. U.S.A. 83*, 1310–1314.
Sassaroli, M., & Rousseau, D. (1987) *Biochemistry 26*, 3092–3098.
Sassaroli, M., Dasgupta, S., & Rousseau, D. L. (1986) *J. Biol. Chem. 261*, 13704–13713.
Sato, F., Shiro, Y., Sakaguchi, Y., Suzuki, T., Iizuka, T., & Hayashi, H. (1990) *J. Biol. Chem. 265*, 2004–2010.
Srajer, V., Schomaker, K. T., & Champion, P. M. (1986) *Phys. Rev. Lett. 57*, 1267–1270.
Srajer, V., Reinisch, L., & Champion, P. M. (1988) *J. Am. Chem. Soc. 110*, 6656–6669.
Stein, D. L., Palmer, R. G., van Hemmen, J. L., & Doering, C. R. (1989) *Phys. Lett. A136*, 353–357.
Steinbach, P. J. (1990) Ph.D. Dissertation, University of Illinois at Urbana–Champaign.
Stetzkowski, F., Banerjee, R., Marden, M. C., Beece, D. K., Bowne, S. F., Doster, W., Eisenstein, L., Frauenfelder, H., Reinisch, L., Shyamsunder, E., & Jung, C. (1985) *J. Biol. Chem. 260*, 8803–8809.
Young, R. D., & Bowne, S. F. (1984) *J. Chem. Phys. 81*, 3730–3737.
Zallen, R. (1983) *The Physics of Amorphous Solids*, John Wiley & Sons, New York.
Zwanzig, R. (1988) *Proc. Natl. Acad. Sci. U.S.A. 85*, 2029–2030.

Properties of 2′-Fluorothymidine-Containing Oligonucleotides: Interaction with Restriction Endonuclease *Eco*RV

David M. Williams, Fritz Benseler, and Fritz Eckstein*

Abteilung Chemie, Max-Planck-Institut für Experimentelle Medizin, Hermann-Rein-Strasse 3, D-3400 Göttingen, FRG

Received October 18, 1990; Revised Manuscript Received December 19, 1990

ABSTRACT: 2′-Fluorothymidine (T_f) was synthesized via an improved procedure with (diethylamino)sulfur trifluoride. The compatibility of the analogue with DNA synthesis via the phosphoramidite method was demonstrated after complete enzymatic digestion of the oligonucleotides $d(T_{f_{11}}T)$ and $d(T_{f_3}T)$, the sole products of which were 2′-fluorothymidine and thymidine in the expected ratio. The 2′-fluorothymidine was also incorporated into the *Eco*RV recognition sequence (underlined), within the complementary oligonucleotides d(CAAACCGATATCGTTGTG) and d(CACAACGATATCGGTTTG). Thermal melting characteristics of these duplexes showed a significant decrease in stability only when both of the thymidine residues in one of the strands were replaced. In contrast, when all of one strand of a duplex contained 2′-fluorothymidine, as in $d(T_{f_{11}}T)\cdot d(A_{12})$, a substantially higher T_m and cooperativity of melting was observed relative to the unmodified structure. *Eco*RV cleaved a duplex that contained a 2′-fluorothymidine at the scissile linkage in each strand at two-thirds of the rate obtained for the unmodified structure. A duplex containing two 2′-fluorothymidine residues in one strand and none in the other was cleaved at one-third of the rate in its unsubstituted strand, whereas the cleavage rate was reduced to 22% in its modified strand.

The differences in both the structure and the properties of ribo- and deoxyribonucleosides and their polymers may be attributed to the nature of the 2′-substituent, –H or –OH. Thus, RNA exists almost exclusively in the A-form in which the ribose moiety exhibits a 3′-endo (*N*) conformation (Saenger, 1984). In contrast, DNA most commonly displays a 2′-endo (*S*) sugar conformation although under certain conditions (in A- and Z-DNA) the 3′-endo conformation is adopted (Saenger, 1984). These differing structural preferences result in the ability of several drugs such as netropsin (Kopka et al., 1985) to recognize and bind exclusively within the minor groove of the B-DNA double helix and also the highly specific cleavage of double-stranded DNA by type II restriction endonucleases (Maass, 1987).

0006-2960/91/0430-4001$02.50/0